POLITECNICO
MILANO 1863

SCUOLA DI INGEGNERIA INDUSTRIALE
E DELL'INFORMAZIONE

Analysis and Modelling of a Latent Thermal Energy Storage for Energy Systems

Tesi di Laurea Magistrale in
Energy Engineering - Ingegneria Energetica

Author: **Marco Ballatore**

Student ID: 992512
Advisor: Prof. Luca Davide Marocco
Co-advisors: Dr. Hannah Romberg
Academic Year: 2022-2023

Abstract

The utilization of Latent Thermal Energy Storage (LTES) in energy systems has gained significant attention due to its potential for improving energy efficiency and enhancing the flexibility of thermal energy management. However, the accurate modelling of LTES and its integration into wider system simulations remain a challenge. This master thesis aims to develop simplified modelling approaches for LTES for dynamic simulations, with an acceptable level of accuracy, to facilitate its integration into larger-scale system simulations. The ultimate objective is to investigate control strategies that optimize the performance of heat pump systems that employ LTES.

The first part of this research involves a comprehensive review of the existing literature on LTES and heat pump systems, focusing on the key factors affecting the storage behavior and the associated modelling techniques. The review will establish a theoretical foundation for the subsequent modelling development.

Different analysis on modelling approaches are carried out to establish the most suitable one, starting from the concentrated parameter Biot assumption validation and moving towards the phase change material (PCM) domain discretization. The ultimate modelling approach analyzes the heat transfer inside the storage by computing the energy exchange between the heat transfer fluid (HTF) and the PCM, and the heat transfer inside the PCM trough the enthalpy approach computed with a finite difference implicit scheme. The enthalpy approach is then improved by incorporating thermal conductivity enhancement factors during the phase transition and liquid phase to account for natural convection. The factors are computed with correlations that take into account the intensity of natural convection through the Rayleigh number that are determined with the auxiliary of CDF simulations carried in Ansys Fluent.

Once the model is validated, the thesis will investigate the behaviour of the storage in heat pump systems for simulations characterized by longer times. The purpose is to investigate the charging and dishcargin times of the storage, through fundamental parameters such as the state of charge (SOC).

The outcomes of this research will provide valuable insights into the modelling of LETS

and its integration into wider heat pump system simulations. The simplified modelling approaches developed in this thesis will enable efficient analysis and design of LTES-based systems. Additionally, the investigation of control strategies will contribute to the development of intelligent and energy-efficient control algorithms for LTES-integrated heat pump systems.

Keywords: latent thermal energy storage, LTES, CFD, heat pump systems, modelling, Modelica, Ansys Fluent, simplified approaches, system integration, energy efficiency, optimization.

Abstract in lingua italiana

L'utilizzo di sistemi di stoccaggio energetico a calore latente nei sistemi energetici ha guadagnato particolare attenzione negli ultimi anni grazie al potenziale di miglioramento dell'efficienza energetica e flessibilità nella gestione dell'energia termica. Tuttavia, la modellazione accurata di tali sistemi e la loro integrazione in sistemi più ampi rimane una sfida. Questa tesi di laurea mira a sviluppare approcci di modellazione semplificati per simulazioni dinamiche, con un livello accettabile di accuratezza, per facilitare l'integrazione in un sistema su scala più ampia. L'obiettivo finale è quello di indagare strategie di controllo che ottimizzino le prestazioni dei sistemi energetici che utilizzano sistemi di stoccaggio a calore latente. La prima parte di questa ricerca prevede una revisione completa della letteratura esistente sui sistemi di stoccaggio e la loro integrazione in pompe di calore, concentrandosi sui fattori chiave che influenzano il comportamento di accumulo e le tecniche di modellizzazione associate. La revisione stabilisce una base teorica per il successivo sviluppo modellistico. Vengono effettuate diverse analisi sugli approcci di modellazione per stabilire quello più adatto, partendo dall'analisi a parametri concentrati tramite l'ipotesi Biot, fino la discretizzazione del dominio e risoluzione del problema tramite uno shcema a differenze finite. Il modello finale analizza il trasferimento di calore all'interno del sistema calcolando lo scambio termico tra il fluido termovettore e il materiale di stoccaggio, e il trasferimento di calore all'interno del materiale stesso attraverso l'approccio entalpico calcolato con uno schema implicito alle differenze finite. L'approccio entalpico viene quindi migliorato incorporando un aumento fittizio della conduttività termica durante la transizione di fase per tenere conto della convezione naturale. I fattori correttivi sono calcolati con correlazioni che tengono conto dell'intensità della convezione naturale attraverso il numero di Rayleigh. I fattori correttivi sono determiati con l'ausilio di simulazioni CDF effettuate in Ansys Fluent. Il modello è poi validato sperimentalmente con uno studio ricavato da letteratura scientifica, per poi essere insertio in un sistema a pompa di calore. Lo scopo è quello di verificare il comportamento del sistema in un'applicazione realsitica, e indagare i tempi di carica e scarica tramite parametri fondamentali quali lo stato di cairica.

Parole chiave: sistema di stoccaggio a calore latente, CFD, pompa di calore, modellistica, Modelica, Ansys Fluent, approcci semplificati, integrazione di sistema, efficienza energetica, ottimizzazione.

Contents

Abstract **i**

Abstract in lingua italiana **iii**

Contents **v**

Introduction **1**

1 State of The Art **3**
1.1 Energy Storage Technologies . . . 3
1.1.1 Electrochemical Storage . . . 3
1.1.2 Pumped Hydro Energy Storage (PHES) . . . 4
1.1.3 Compressed Air Energy Storage (CAES) . . . 5
1.1.4 Hydrogen Energy Storage . . . 5
1.1.5 Thermal Energy Storage (TES) . . . 6
1.2 Thermal Energy Storage in Heat Pump Systems . . . 7
1.3 Applications of PCM and Latent Energy Thermal Storage . . . 9
1.4 Existing Work on Modelling Latent Thermal Energy Storage . . . 11
1.4.1 Mathematical Modelling of LTES . . . 12
1.4.2 Dynamic Modelling of LTES . . . 17
1.5 Research Gap . . . 19

2 Modelling Approaches to Phase Change **21**
2.1 Phase Change Physics . . . 23
2.1.1 Single Slab Lumped System Modelling . . . 24
2.1.2 PCM Domain Discretization . . . 26
2.1.3 PCM Properties Variability with Temperature . . . 28
2.1.4 Initial and Boundary Conditions . . . 31
2.2 Model Assumptions Validation . . . 31

2.2.1 CFD Setup Specifications . . . 32
2.2.2 Slab Dimensions Impact on CFD Results . . . 33
2.2.3 Fictive Thermal Conductivity Model . . . 37
2.2.4 Mesh Independence Analysis . . . 39
2.2.5 Final Internal PCM Heat Transfer Model . . . 41

3 Heat Interaction between HTF and PCM 43
3.0.1 Channel Geometry . . . 43
3.0.2 Fluid-Dynamic Analysis of HTF Flow . . . 44
3.0.3 Boundary and Initial Conditions . . . 48
3.0.4 Boundary Layer Analysis . . . 49
3.0.5 PCM Containment Model . . . 53

4 Modelica Implementation and Model Validation 57
4.0.1 Modelica Libraries . . . 57
4.0.2 Single Slab Model . . . 59
4.0.3 HTF Heat Transfer Model . . . 60
4.0.4 Slab Encapsulation Model . . . 62
4.0.5 Multiple Slabs Model Extension . . . 62
4.0.6 Storage Container Model . . . 64
4.0.7 Full Model . . . 65
4.0.8 State Of Charge . . . 65
4.0.9 Integration in Heat Pump System . . . 67
4.0.10 Experimental Validation . . . 69

5 Conclusion 73

6 Bibliography 75

Introduction

As the world faces increasing concern over climate change and environmental sustainability, there is a pressing need for transition towards clean and renewable energy technologies. Governments around the world have set ambitious targets to reduce greenhouse gas emissions, such as the Paris Agreement to limit Earth's temperature increase to 1.5°C above pre-industrial levels. The energy transition involves the shift from a conventional fossil fuel based energy system to a more diversified mix that heavily relies on renewable energy. In the last years, renewable energy technologies such as solar and wind have shown a significant increase in efficiency as well as decrease in cost, making them increasingly more competitive with conventional sources. However, the intermittency and low flexibility make their integration in the national grids and the satisfaction of electricity demand difficult. One of the key solutions to address this challenge is represented by energy storage. Energy storage technologies allow to store excess energy from renewable sources during times of high production and provide it when the generation is low. Furthermore, they provide ancillary services to the electric grid, such as supply-demand balance and frequency regulation.

Among different storage technologies, Latent Thermal Energy Storage (LTES) has gained significant attention in the last years. This kind of storage uses latent heat of phase change materials (PCM) during phase change to store and release thermal energy. LTES presents a wide range of applications, such as controlling the temperature of photovoltaic panels, store thermal energy of concentrated solar power plants, heat recovery, HVAC systems, heat pumps integration and even space applications. The integration of renewable sources in the energy mix requires the development of efficient control strategies. The development of a storage model in object-oriented sofwtares such as Modelica emerges as a crucial tool. The intermittency of renewable energy sources demands flexible energy storage solutions that can adapt to varying supply and demand conditions. The ability of a dynamic model to simulate complex interactions between components provides a comprehensive understanding of their behavior within larger energy systems. The dynamic modelling approach allows for the development of precise and adaptable control strategies that optimize energy flows, storage utilization, and system stability. Ultimately, the

incorporation of Modelica-based dynamic storage models holds the potential to enhance the efficiency, reliability, and sustainability of modern energy systems while facilitating the transition towards a cleaner and more resilient energy future.

1 | State of The Art

In the pursuit of sustainable energy solutions, the landscape of energy storage technologies has witnessed remarkable advancements. Among these, thermal energy storage stands out as a versatile and effective approach. Thermal storage technologies enable the efficient capture and release of thermal energy, addressing the intermittency of renewable sources and enhancing overall energy system flexibility. These systems encompass a range of technologies, from sensible heat storage that employs simple fluids like water, to more innovative methods such as thermochemical and latent heat storage. As we delve into the state of the art of energy storage, the discussion will place a spotlight on the significance, progress, and potential applications of latent thermal energy storage in shaping the future of resilient and sustainable energy systems.

1.1. Energy Storage Technologies

Energy Storage Technologies play a crucial role in the energy transition, enabling the storage and release of energy, helping to reduce the problem of intermittency of renewable energy sources, providing grid stability and back up power during times of high demand or grid outages. In this paragraph, a brief overview of energy storage technologies is presented.

1.1.1. Electrochemical Storage

It is the most widely used energy storage system. It is mainly categorized into two types: battery energy storage (BES) systems, in which charge is stored within the electrodes, and flow battery energy storage (FBES) systems, in which charge is first stored within a fuel and then externally fed on to the surface of the electrodes [1].

- Battery Energy Storage (BES)

  Batteries are electrochemical devices that convert chemical energy into electrical energy. They are composed of a number of cells, each of which has three basic

components: two electrodes, namely, an anode and a cathode, and an electrolyte. They are broadly categorised into two groups: primary and secondary. Primary batteries are intended to be single-use batteries, with the chemical that, once consumed, cannot be recharged. Secondary batteries, on the other hand, are designed to be recharged [2]. Secondary batteries are classified as lead-acid, lithium-ion, nickel-cadmium, sodium sulphur, sodium-ion, and metal air batteries, depending on the material of the electrodes and electrolyte. BES systems present several advantages, such as flexibility, fast response, high round-trip efficiency, modularity and scalability, making the technology suitable for grid stabilization, load balancing and mitigating the intermittency of renewable energy generation. Nonetheless, the disadvantages are mainly represented by a lower energy density compared to other technologies, aging, environmental and safety concerns due to intense and laborious manufacturing process and high investment costs.

- Flow Battery Energy Storage (FBES)

  Flow batteries consume two electrolytes that are stored in separate external tanks, with a microporous membrane that separates both the electrolytes but allows only selected ions to pass through it, producing current [3]. FBES systems are classified into two types: reduction-oxidation flow battery and hybrid flow battery. In the first case, all the electroactive materials are dissolved in a liquid electrolyte, whereas in the second, one or more electroactive materials are deposited in the electrolyte [4].

1.1.2. Pumped Hydro Energy Storage (PHES)

PHES systems are the most widely implemented energy storage systems with a huge energy capacity, long storage period and high efficiency [5]. A typical PHES system consists of two large reservoirs located at different elevations, a unit to pump water from the lower reservoir to the higher reservoir, and a turbine to generate electricity as water flows downwards from the upper reservoir to the lower reservoir. During off-peak hours, the electrical energy from the power source is turned into mechanical energy, which is then converted into potential energy by pumping and storing water from lower reservoir to the higher reservoir through pumping mode. During peak hours, the stored water from the upper reservoir is released back into the lower reservoir, rotating the turbines and generating electricity [5]. By transferring water between two reservoirs at different elevations, it stores and generates energy in the form of potential energy. The volume of water stored in the reservoirs and the difference in elevation between them determine the amount of storable energy [6]. These systems are characterized by high efficiencies up to

85%, huge amounts of storable energy, long lifetime up to 50 years, lower environmental impact compared to other technologies and black start capability, allowing for the grid to restart after a blackout. The disadvantages of the technology are surely the geographical constraint of having two water reservoirs at different elevations to be exploited, high investment costs, non negligible land use and higher response times compared to other technologies due to the need to shift from charging to discharging mode.

1.1.3. Compressed Air Energy Storage (CAES)

CAES is an energy storage technology that stores energy by compressing air. The amount of stored energy depends on the volume of the storage container as well as the pressure and temperature at which the air is stored [3]. CAES was developed as an alternative to PHES and has proven to be a promising method of energy storage due to its high reliability, economic feasibility, and low environmental impacts. A typical CAES system consists of the following five major component: a motor that drives a compressor, a multi-stage compressor that compresses the air, a container or cavity for storing compressed air, which can be underground caverns or porous reservoirs, a turbine train that includes both high and low pressure turbines and a generator which returns electrical energy to the grid. During off-peak hours, surplus electricity is used to drive the motor, generating mechanical energy and driving the multi-stage compressor. The compressor raises atmospheric air pressure, which is then stored in the underground cavern. During peak hours, the compressed air stored in the cavern is used to drive the turbines, which convert compressed air energy into mechanical energy, which is then used to drive a generator that generates electricity [7]. This technology can store significant amount of energy with high efficiencies up to 70%, has long lifespan and, by compressing the air underground, it has the advantage of being applicable to many different sites. Nonetheless, it comes with high investment costs and air pollution due to combustion, since in many cases natural gas is burnt to heat up the compressed air before expansion.

1.1.4. Hydrogen Energy Storage

Hydrogen is regarded as an ideal energy carrier as it is clean, and a carbon-free chemical energy carrier [8]. It can be produced from water via electrolysis or directly from sunlight using photocatalytic water splitting. A typical hydrogen energy system comprises three major components: a hydrogen generation unit such as an electrolyser to convert the electrical energy input into hydrogen, a hydrogen storage system and a hydrogen energy conversion unit, such as a fuel cell, to convert the stored chemical energy in the hydrogen back to electrical energy. When there is excess power during the charging process, hy-

drogen is produced from water via electrolysis and stored in a storage tank. During peak hours, when power availability is limited, electricity is generated from stored hydrogen using fuel cells. An electrolyser uses electrolysis to break down water into hydrogen and oxygen. The oxygen is then released into the atmosphere, while the hydrogen is stored in the storage tank. The technology is characterized by high energy density, carbon free operation and the possibility to store energy for long periods of time without degradation, making it suitable for seasonal storage. The disadvantages are represented by low energy efficiency due to many processes involved, infrastructure need, storage and transport issues, high costs and scaling difficulties.

1.1.5. Thermal Energy Storage (TES)

TES systems are specially designed to store thermal energy by cooling, heating, melting, condensing, or vaporising a substance. Depending on the operating temperature range, the materials are stored at high or low temperatures in an insulated repository; later, the energy recovered from these materials is used for various residential and industrial applications, such as space heating or cooling, hot water production, or electricity generation, depending on the operating temperature range. TES systems are utilised for a variety of purposes, including industrial cooling below –18 °C, building cooling between 0 and 12 °C, heating buildings between 25 and 50 °C and industrial heat storage over 175 °C. TES systems are divided into two categories: low temperature thermal energy storage systems and high temperature thermal energy storage systems, based on the operating temperature of the energy storage material in relation to the ambient temperature. There are three main types of TES systems in use:

- Sensible Thermal Energy Storage (STES)

  SHS is the most widely deployed TES system. It stores thermal energy by raising the temperature of a solid or liquid without affecting its phase [9]. The technology is cheap and very simple. Nonetheless, it has low energy density and is subjected to non negligible thermal losses. Due to the low energy density, it is mainly employed for residential and low temperature applications.

- Latent Thermal Energy Storage (LTES)

  LTES system utilises the amount of heat absorbed or released when the storage material undergoes a phase change [10]. The ability of storage material to undergo phase change at almost constant temperature is critical to the performance of the

system. Due to the very small volumetric change that makes the technology more practical and easily applicable, phase change from solid to liquid is usually considered. As the energy in the form of heat is added to the material, the consequence is an increase in temperature (sensible heating) or a change of phase (latent heating). The heat absorbed during the phase transition is known as latent heat of fusion. LTES have high energy density and are able to store a high percentage of thermal energy at almost constant temperature, which makes it suitable for many applications. The thermal losses are lower than for STES. Nonetheless, the technology has a higher cost.

- Thermochemical Energy Storage (TcES)

  TcES is a method of indirectly storing thermal energy. Heat is not directly stored as in STES or LTES, but is absorbed and released during dissociation/association of molecular bonds in an entirely reversible chemical reaction [10]. It stores thermal energy by utilising the enthalpy of reaction. The amount of heat stored depends on the type and amount of storage material, the enthalpy of the reaction, and the degree of conversion. TcES has the great advantage of having null thermal losses and a very high energy density. It can also be operated at very high temperature, making it suitable also for industrial applications. Nonetheless, it has high investment and operating costs.

1.2. Thermal Energy Storage in Heat Pump Systems

The integration of thermal storage in heat pump systems enables energy efficiency, load management, and system performance. By incorporating thermal storage, heat pump systems can better align energy supply and demand, allowing for the utilization of excess energy during off-peak periods for heating or cooling purposes. Furthermore, thermal storage enhances the overall efficiency of heat pump systems by allowing operations at optimal conditions, as the stored energy can be used during times of lower ambient temperature or when renewable energy generation is low. By combining heat pumps with thermal storage, buildings and facilities can achieve greater energy savings, reduce operating costs, and contribute to higher sustainability and flexibility.
Previous studies have investigated the benefits of integrating thermal storage in heat pump systems.
Wei et al. [11] analyzes the performance of a solar assisted heat pump system with thermal energy storage in Beijing, China. An optimal design of heat pump, storage and solar

collectors as well as optimal operation mode based on economic evaluation is proposed. The results show that with the optimal heat storage ratio of 50% the rated capacity of the system could be reduced by 16.7%, leading to a reduction in total annual cost of 26.5%.
The performance of a standard heat pump can be significantly increased when coupled with thermal storage. [12] reports the results of 15 studies conducted on integrated systems. The investigated systems present a heating capacity withing 5 kW and 10 kW. Most of the reviewed papers present COP values up to four, higher than the corresponding ones for the systems without TES. [13] investigates the benefits provided to a solar assisted heat pump in cold regions when CaCl2·6H2O/Expanded Graphite composite phase change materials are used as the heating source of the system. This allows to improve the evaporation temperature and assures high performance operation. Results show that the average COP and exergy efficiency of the solar assisted heat pump increase respectively of 70% and 67%. Also, the time required for heating water from 15°C to 55°C decreases of about 50%.
The use of thermal storage in heat pump systems is not only limited to energy supply purposes. One key problem in heat pumps is represented by the forming of ice layers on the evaporator, which requires defrosting. As reported by Ermel et al. [12], the most common method is to temporally reverse the thermodynamic cycle so that the external unit can function as a condenser. This solution results in a significant decrease of the COP. An alternative solution is investigated by Minglu Qu et al. [14], that proposes a novel thermal energy storage reverse based cycle defrosting method for cascade air source heat pumps. The system is able to provide heat to the defrosting cycle through a latent thermal energy storage, while still supplying heat to the indoor space. The results show that the defrosting time is shortened by 64.3% and the energy consumption by 30.3% when compared to standard defrosting methods. Another solution has been proposed by Long et al. [15] which consisted in storing the heat dissipated by the compressor and use it for the defrosting cycle while still providing heat to the indoor space. To do so, a latent thermal energy storage is used. Results show that the COP increases only by 1.4%, but the defrosting time decreases by 65%.
The integration of TES in heat pump systems can present many benefits, other than system performance enhancing. Cuncha et al. [16] performs a comparison between two space heating systems that use air source heat pumps. One is integrated with a latent thermal energy storage with encapsulated PCM spheres in a packed bed, while the other uses a conventional boiler. The results from the simulation show a potential for carbon emissions reduction of 23% in the UK.
One of the biggest advantages of TES is represented by the possibility of load shifting. This characteristic is crucial since the energy transition moves towards a scenario where

photovoltaic and wind energy represent the biggest share for power production. In this situation, the electrification and sustainable development of the residential sector plays a relevant role. DeValeria et al. [17] performs a detailed analysis on the hourly, daily and yearly operation of a cluster of off-grid buildings that relies entirely on photovoltaic for power generation, and stored energy in thermal and chemical storage systems. The results show that thermal storage coupled with the chemical one is able to reduce the solar power installation by 40%. Furthermore, TES represents a promising solution for grid stability purposes. As the world moves from a centralized energy system to a decentralized one with high level of distributed power generation from photovoltaic and wind energy sources, problems of grid stability such as overload may occur. TES can be used to store surplus energy production form renewable sources. Finally, TES can help achieving significant operational cost reductions. It can be employed to shift thermal loads to periods in which electricity generation is lower, providing a benefit to the consumer.

1.3. Applications of PCM and Latent Energy Thermal Storage

LTES is a type of thermal storage that exploits latent heat of phase transition to store large amount of thermal energy in a very narrow temperature range. The materials employed are called phase change materials (PCM). Phase change is a process that results in the change of the state of aggregation of the material: solid, liquid or vapor. Most LTES exploit the phase transition from solid to liquid and liquid to solid for practical reasons. In this case, in fact, there is a small change in volume that generally does not overcome 10%. After the phase change is completed, the storage device is able to store more energy as sensible heat.

According to [18] LTES can be divided into direct and indirect systems based on the interaction between the heat transfer fluid (HTF) and the PCM. In direct systems, heat transfer is facilitated by direct contact between HTF and PCM. Conversely, indirect systems separate the HTF and PCM with a solid heat transfer interface.

PCM can be classified based on their chemical nature and temperature range applications. As reported by Khan et al. [19], PCMs can be divided into organic (e.g paraffins and fatty acids), inorganic (e.g salt hydrates and metallic) and eutectics (mixture of organic-organic, inorganic-inorganic and organic-inorganic materials). Each type of material presents its own characteristics, strengths and limitations. However, organic PCMs are generally used for LTES applications. They are made up of mixture of alkalines of type CnH2n+2 and their increase in chain length ensures a higher melting point and latent heat (between 60

to 269 J/kg). Furthermore, they are chemically stable, don't present tendency to super cooling, have low vapour pressure and are commercially available at affordable price.
Regarding the operating temperatures, according to Elias et al. [20], there are four temperature ranges based on their applications: low temperature (-20°C to +5°C) used for domestic and commercial refrigeration, medium-low temperature (+5°C to +40°C) used for cooling and heating in buildings, medium temperature (+40°C to +80°C) used for solar based heating, hot water and electronics and high temperature (+80°C to +200°C) used for absorption cooling, heat recovery and power production.
One of the biggest problems regarding PCMs is represented by the very low thermal conductivity (around 0.2 W/mK), which make the heat exchange with the HTF challenging. For this reason, the correct design and configuration of the storage represents a crucial aspect to ensure optimal performance.
The choice for PCM is often difficult and strongly depend on the application. The material should, in general, meet the following characteristics, as reported in Veerakumal et al. [21]:

- Melting temperature must be in the operational range.
- High latent heat.
- High thermal conductivity.
- High density.
- Low volume change during phase transition.
- Low degree of super cooling.
- Low corrosion to construction materials.
- Low degradation.
- Chemically stable.
- Non toxic and non flammable.
- Easily available.
- Cost effective.

LTES can be employed in a wide range of applications, such as temperature regulation for batteries and photovoltaic panels, spacecraft hardware thermal control, textile, waste heat recovery for the industry, building and residential, agriculture and even fuel cells.
Moraga et al. [22] performes a numerical study on the cooling process of a Li-Ion battery used in solar vehicles, and compared the results with the case of battery without PCM.

The study shows that the cooling process that employs PCM is able to reduce the maximum temperature of up to 23.2 K with respect to the standard case.
Khateeb et al. [23] performs an experimental analysis and compares the results of 4 different modes of heat dissipation of a Li-Ion battery for an electric scooter. The modes considered were natural convection cooling, presence of aluminum foam heat transfer matrix, employment of PCM and combination of aluminum foam and PCM. The results show that natural convection cooling is the less efficient mode. The aluminum foam heat transfer matrix is able to reduce the temperature raise in the battery but becomes inefficient when operated in high ambient temperature conditions that typically occur during summertime. The employment of PCM can bring significant temperature reduction, but the low thermal conductivity results in slow heat dissipation, causing unfavorable thermal environment for the battery. Overall, the use of combined aluminum and PCM can bring a temperature drop of about 50% with respect to the case of no thermal management. Furthermore, it allows a more uniform temperature distribution, which is crucial for the efficient operation of the battery cells.
Young Kim et al. [24] suggests a new spacecraft thermal control hardware composed of two parallel channels working for heat pipe (HP) and solid-liquid PCM for the high heat dissipating purpose. The comparison of the results with the case without PCM shows that the HP-PCM device is able to redistribute the temporal peak heat around a whole orbit period thanks to the alternating melting and freezing of the PCM. This also allows to alleviate the maximum and minimum temperatures. A significant data shows that by just employing 47 g of PCM, the device is able to reduce the temperature change by 28°C.

1.4. Existing Work on Modelling Latent Thermal Energy Storage

This section aims to provide a comprehensive overview of existing modelling approaches for latent thermal energy storage. Modelling plays a crucial role in the design, optimization, and performance evaluation of LTES systems. By understanding the different modelling techniques, their strengths and limitations, informed decisions can be made to advance LTES technologies. The section is divided in two subsections: in the first one, mathematical modelling for the heat transfer mechanism inside the storage from literature is presented, while the second focuses on the implementation of dynamic models in object-oriented programs.

1.4.1. Mathematical Modelling of LTES

Phase transition involves the change in the thermodynamic properties of the material, both in time and space. This makes the mathematical modelling a crucial aspect to be considered. The analysis of heat transfer problems involving solidification and melting, called moving boundary problems in scientific literature, is particularly complicated to model since the solid-liquid interface moves at different speeds depending on the rate of absorption or release of the latent heat. This implicates that the position of the interface is not known at priori and constitutes part of the solution. The solution of the problem is obtained by solving the continuity, momentum and energy equations. Several mathematical modelling approaches have been previously investigated and will be presented in this section.

If the PCM is not pure but is a mixture of different materials, then the phase change does not occur at constant temperature but over a narrow temperature range. In this case, as reported in [25] it is appropriate to consider the energy equation in terms of enthalpy, which if the advective movements in the inner of the liquid are disregarded, is expressed mathematically as:

$$\rho\frac{\partial h}{\partial t} = \frac{\partial^2(KT)}{\partial x^2} + \frac{\partial^2(KT)}{\partial y^2} + \frac{\partial^2(KT)}{\partial z^2} \tag{1.1}$$

This is noted as the Enthalpy Model, and the solution of the equation requires the knowledge of the dependency of enthalpy on temperature as well as the function relating the thermal conductivity of the PCM to its temperature. The strength of this model is that it is applicable to all three phases, the temperature is determined at every point and the thermophysical properties are defined for every temperature that is reached by the material. Nonetheless, the equation fails in considering the transport terms in the energy equation due to the motion of the fluid during phase change.

Gong et al. [26] developed a finite-element model to simulate the cyclic thermal process occurring in a shell and tube latent heat thermal storage exchanger. This exchanger consists of a tube, in which the HTF flows, that is surrounded by an external co-axial cylinder made up of PCM The objective of this model is to investigate the characteristics of two operation modes, which are named mode 1 and mode 2. In mode 1 the hot and cold fluids (for charge and discharge process, respectively) are introduced from the same end of the tube where as in mode 2 the hot and cold fluids are introduced from different ends of the tube. The assumptions made for the mathematical description of the model are:

- The heat-transfer fluid is incompressible and viscous dissipation is negligible.
- The fluid flow is radially uniform and the axial velocity is an independent parameter.

- Thermal losses through the outer wall of the PCM are negligible.
- Heat transfer in the PCM is conduction controlled.
- The densities of the solid and liquid phases of the PCM are equal.

The energy transfer is considered for two different zones: the HTF and the PCM. Two governing equations for the energy transfer are then developed:

$$\rho_F c_F \left(\frac{\partial T_F}{\partial t} + v \frac{\partial T_F}{\partial x} \right) = \frac{4h_c}{D} \left(T_P - T_F \right) + K_F \frac{\partial^2 T_F}{\partial^2 x} \tag{1.2}$$

for the HTF

$$\frac{\partial H_P}{\partial t} = \left(\frac{1}{r} \right) \frac{\partial}{\partial r} \left(K_P r \frac{\partial T_P}{\partial r} \right) + \frac{\partial}{\partial x} \left(K_P \frac{\partial T_P}{\partial x} \right) \tag{1.3}$$

for the PCM.

The instantaneous temperature distribution in the PCM is obtained using standard Galerkin finite-element method and a three time-level scheme incorporating lumped heat capacity is used to accomplish the time discretization of the equation. The magnitude of the cumulative energy charged or discharged Q is calculated as a function of time for each charge or discharge period. This calculation is made by computing the enthalpy of the PCM at each time increment, using the solid PCM at its fusion temperature as the reference state, and then subtracting the enthalpy of the PCM at the beginning of the period.
Saman et al. [27] proposed a phase-change energy storage system consisting of sections of different materials with different melting temperature for air conditioning applications. The PCMs are placed in thin flat plate containers and air is passed in series through gap in between them. The freezing and melting processes of the PCM and heat transfer in the flowing fluid are unsteady two-dimensional problems. To develop a mathematical model for the proposed problem, the following assumptions are made:

- PCM supercooling effects are neglected, axial conduction of the PCM and fluid are negligible.
- The heat capacity of the fluid is ignored.
- The quasi-static assumption is applied to convective heat transfer in the air passages, i.e. transient convection is considered as a series of steady-state problems.
- The heat capacity and axial conduction of the container walls are negligible.
- Natural convection in the liquid portion of PCM is ignored.

On the basis of these assumptions, a mathematical model is developed for the storage system. The heat transfer equation and initial and boundary conditions for a PCM slab are as follows:

$$\frac{\partial T}{\partial t} = \alpha \frac{\partial^2 T}{\partial^2 x_w} \qquad for \quad 0 < x_w < \delta(t) \tag{1.4}$$

$$T_{x_w=0} = T_w \tag{1.5}$$

$$T_{x_w=\delta(t)} = T_m \tag{1.6}$$

$$K \frac{\partial T}{\partial x_w} = \rho h_F \frac{\partial \delta}{t} \qquad for \quad x_w = \delta \tag{1.7}$$

where

$$\delta = 2s\sqrt{\alpha t} \tag{1.8}$$

and

$$\frac{\partial \delta}{\partial t} = \frac{2\alpha}{\delta} s^2 \tag{1.9}$$

where δ is the solid liquid interface of the PCM.
Xu et al. [28] developed a model to analyze the thermal performance of shape-stabilized PCM floor and studied the influence of melting temperature, heat of fusion, thickness of PCM layer and thermal conductivity of PCM on the thermal performance of passive solar buildings by using the enthalpy model. The model takes enthalpy as the only variable instead of temperature and specific heat capacity. In order to simplify the analysis, the following assumptions were made:

- Heat transfer through walls, floor and ceiling is one dimensional.
- Thermo-physical properties of the building material are constant except the specific heat of PCM during melting or freezing process.
- The shape-stabilized PCM plate under surface is thermally insulated.

The governing equations are solved numerically using the Gauss–Seidel method. A fully implicit finite-difference scheme was applied, and the number of grids was checked to ensure accuracy and to eliminate initial errors.
Halawa et al. [29] developed a two-dimensional model considering convection as a dominant mode to analyze the characteristics of a PCM thermal storage unit for roof integrated solar heating systems. The model takes into account the sensible heat transfer at the initial periods of melting and freezing of PCM and the inlet temperature of air is taken well above the melting point of the PCM. The mathematical model employed is based

on enthalpy formulation and calculation of liquid fraction of PCM, sensible and total enthalpies when the PCM is in mushy zone is performed as per Voller [30], which developed a rapid implicit solution technique for the enthalpy formulation of conduction controlled phase change problems. In the initial condition for the PCM melting process, the PCM is taken solid and its temperature is assumed at a certain value below the melting point. For freezing, the PCM is initially liquid and its temperature is assumed at certain value above the melting point. These two situations can be expressed mathematically as:

$$h_{init} = \rho_s c_s \left(T_m - T_{init}\right) \qquad for \;\; melting \tag{1.10}$$

$$h_{init} = \rho_l c_l \left(T_m - T_{init}\right) \qquad for \;\; freezing \tag{1.11}$$

where T_m is the melting temperature of the PCM.
The variation in wall and fluid temperatures along the air passage is taken care by using standard heat-transfer equations, for the duct cross-section at any distance x from the entrance, the following energy balance equation can be written as:

$$m_a c_a \frac{\partial T}{\partial x} = h_x P \left(T_w - T_{a-x}\right) \tag{1.12}$$

The HTF mass flow rate is computed as:

$$m_a = \rho_a U_a A_c \tag{1.13}$$

The heat conducted through the wall to the PCM surface node is:

$$Q_{cond} = K_{wall} A_n \frac{\left(T_{wall} - T_{PCM}\right)}{\Delta y_{wall}} \tag{1.14}$$

To calculate the fluid, wall and PCM node temperatures at any distance from the entrance, the following equations are employed:

$$Q_a = m_a c_a \left(T_{a,in} - T_{a,out}\right) \tag{1.15}$$

$$\frac{\partial H_P}{\partial t} = \left(\frac{1}{r}\right) \frac{\partial}{\partial r} \left(K_P r \frac{\partial T_P}{\partial r}\right) + \frac{\partial}{\partial x} \left(K_P \frac{\partial T_P}{\partial x}\right) \tag{1.16}$$

Bellander et al. [31] developed a mathematical model of the PCM air heat exchanger based on the finite-difference method, where the thermal properties of the material are considered and considerations are taken to different shapes of the specific heat capacity curve and it is shown that the curve will affect the cooling power of PCM heat exchanger. The heat exchanger is modeled as duct with airflow where the PCM has a constant temperature. The equations for the heat balance for an element dx to calculate the power of the heat exchanger are as follows:

$$Q = vA\rho_a c_a \left(T\left(x\right)\right) - T\left(x + dx\right) + PdxU_P \left(T_{PCM} - T\left(x\right)\right) = 0 \tag{1.17}$$

$$Q = vA\rho_a c_a \left(T_{in} - T\left(x\right)\right) = \alpha_P PL \left(T_{in} - T_{PCM}\right) \tag{1.18}$$

where α_P is the fctive heat transfer coefficient defined as:

$$\alpha_P = \frac{vA\rho_a c_a \left(1 - e\left(PU_P L\right) / \left(vA\rho_a c_a\right)\right)}{PL} \tag{1.19}$$

Dwarka et al. [32] presented a mathematical model for comparing the thermal performance of randomly mixed and laminated PCM drywall system. The model was based on implicit enthalpy method and the governing equations for both randomly mixed and laminated PCM systems were solved by finite-difference method. The assumptions made for the model are:

- Both systems contain the same amount of PCM.
- One side of the wallboard is fully insulated.
- Air temperature is constant during the heat recovery and storage processes.
- Initial temperatures are the same through the board.
- There is no energy loss to surroundings.
- There is no convective heat transfer in the liquid phase of PCM.
- All thermophysical properties are constant except the heat capacity.

For analysis of randomly mixed PCM systems the differential energy equation in rectangular coordinates x, y and z is represented as:

$$\frac{\partial}{\partial x}\left(K\frac{\partial T}{\partial x}\right) + \frac{\partial}{\partial y}\left(K\frac{\partial T}{\partial y}\right) + \frac{\partial}{\partial z}\left(K\frac{\partial T}{\partial z}\right) = \rho\frac{\partial h}{\partial t} = \rho\frac{\partial}{\partial t}\int Cdt \tag{1.20}$$

1.4.2. Dynamic Modelling of LTES

In this subsection, the focus is on the implementation of dynamic models of the LTES from literature and their integration in object-oriented programs such as Modelica. It is important to understand how mathematical models such as the ones previously described can properly interact with outer components.
Helmns et al. [33] describes the transfer of the numerical framework of a LTES model to an implementation in a Modelica component and validates it with experimental results. The storage consists of stacked rectangular sections, alternating between flow passages and PCM sections, as shown in Fig 1.1.
Before constructing complex system models, the authors verified Modelica's capability to effectively capture phase change physics in the thermal storage component.
The preliminary model test setup, shown in Fig 1.2 was composed of a connected series of unit cells of finite volume. On one side of these, the primary pump delivered the heat transfer fluid to the heat exchanger at a specified inlet temperature. The working fluid traveled through the series of PCM heat exchanger elements before reaching the outlet.
The preliminary model for a PCM heat exchanger element of the TES device is shown in figure 1.3. This includes two ports on either side that served as inlets and outlets for the working fluid. There are also two temperature sensors, one before and one after the energy transfer. On the working fluid side, the convective heat transfer coefficient was computed by a function that determines its value based on the Reynolds number. A pipe component is inserted in the model to replicate the resistance of the flow channels to the HTF.
The PCM is exposed to a convection boundary, with the flow channel control volume on one side (s = 0) and a symmetry boundary at the centerline of the storage section between flow passages. The thickness of the slab, x, between these two boundaries is defined in the PCM material record. In Modelica, there is the possibility to spatially resolve the PCM unit cell by changing a parameter which dictates the number of nodes. This can be automatically determined by an algorithm based on the thickness and thermal diffusivity of a material slab. The PCM matrix unit cell in the thermal energy storage model used the Modelica conduction component. The algorithm behind this object is the heat diffusion equation with specific internal energy, u, replacing temperature, T, as the independent variable to be determined:

$$\rho c \frac{\partial T}{\partial t} = K \frac{\partial^2 T}{\partial^2 x} \tag{1.21}$$

The full TES model is composed of a series of finite volumes and discretizes the LTES into a number of heat exchanger elements that capture the most basic heat transfer phenomena between the working fluid and PCM. There were a few simplifications in the preliminary

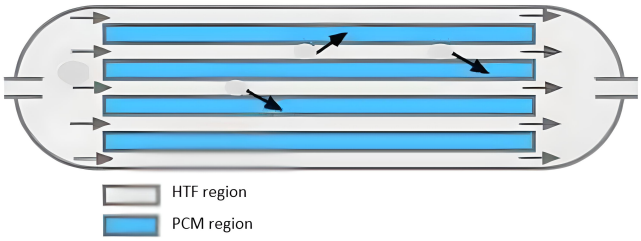

Figure 1.1: Slab LTES

model that we improved with three major enhancements. In the full model, additional thermal mass in the heat exchanger core due to the metal casing that contains the PCM is considered. This mass is most significant around the perimeter of the core. On the top, bottom, and sides, there are aluminum plates that are 5 mm thick. To account for this capacitance, the metal case was added to a perimeter heat exchanger element in the Modelica model as in figure 1.3.

The thermophysical properties of this metal case are specified in a material record. As the material is significantly more conductive than PCM, the metal case unit cell undergoes axial conduction with neighboring nodes in the PCM heat exchanger. It has an insulation boundary to prevent environmental heat losses.

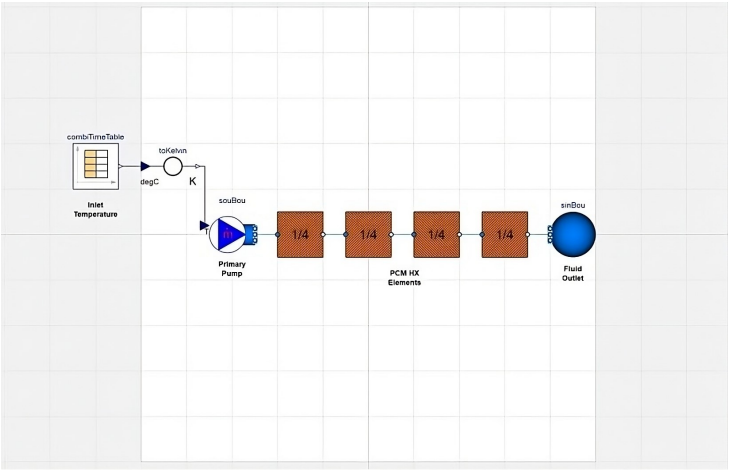

Figure 1.2: Modelica test model

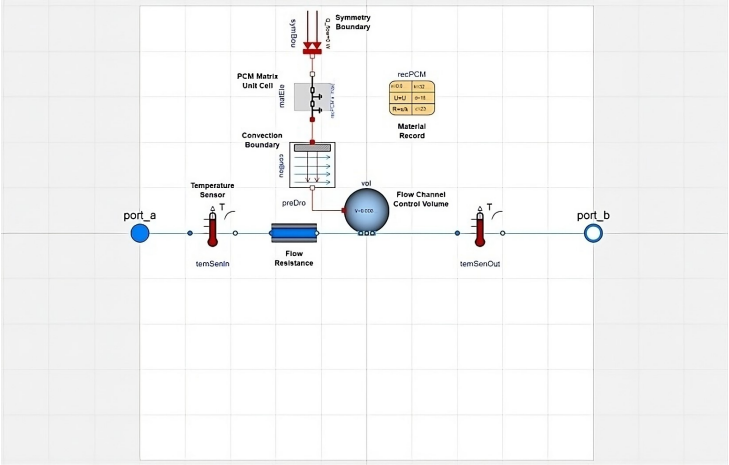

Figure 1.3: Preliminary model

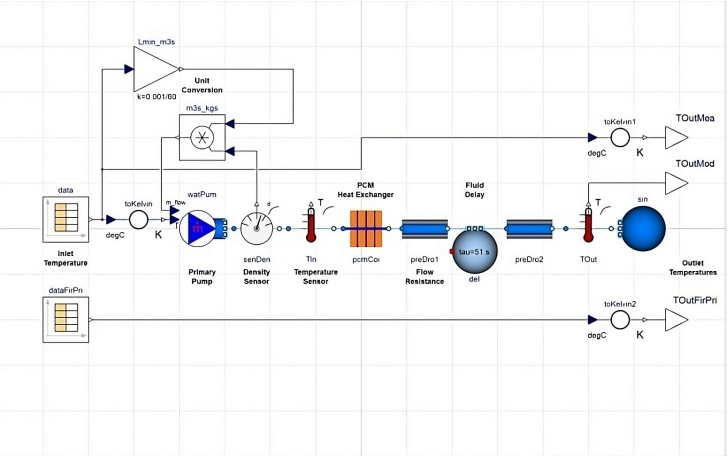

Figure 1.4: Full model

The flow channel is divided axially into pipe segments that are specified as a parameter rather than hard-coded. The full model also accounts for manifolds to divide the flow into parallel elements with a common convection coefficient. There are two outer flow channels and any number of inner flow channels, which is consistent with most rectangular stack PCM heat exchanger designs. The model user can specify the number of sequential and parallel pipes as parameters.

1.5. Research Gap

A significant research gap exists in the domain of latent thermal energy storage modelling, as a substantial portion of the existing literature primarily concentrates on isolated models without a strong emphasis on their integration within broader energy systems for extended simulations. While numerous studies have successfully explored the fundamen-

tal characteristics and performance of latent thermal energy storage materials, it still remains a limited focus on the development of models that can seamlessly integrate into larger dynamic environments, such as the Modelica platform, and operate over extended times. The current body of research often lacks the consideration of real-world complexities and the ability to simulate latent thermal energy storage behavior within the context of dynamic energy systems. Bridging this gap is crucial for advancing the practical deployment of latent thermal energy storage technologies, enabling accurate long-term simulations and optimization of their integration in complex energy systems, and thereby contributing to the development of efficient and sustainable energy strategies.

2 | Modelling Approaches to Phase Change

LTES involves storing thermal energy through the phase change of PCM. As previously mentioned, the critical aspect of the materials that are usually employed is represented by the extremely low thermal conductivity. This feature makes the thermal interaction between the PCM and the HTF challenging. Furthermore, since there is a change of state from solid to liquid, containment must be employed to assure no spilling of the PCM. This accounts for additional thermal resistance to the heat transfer. For these reasons, the optimal design of the storage is a key aspect for achieving acceptable performances. There are different design configurations for LTES, and each of them aims at maximizing the exchange area between PCM and HTF. The most employed designs are the following:

- Slab LTES.

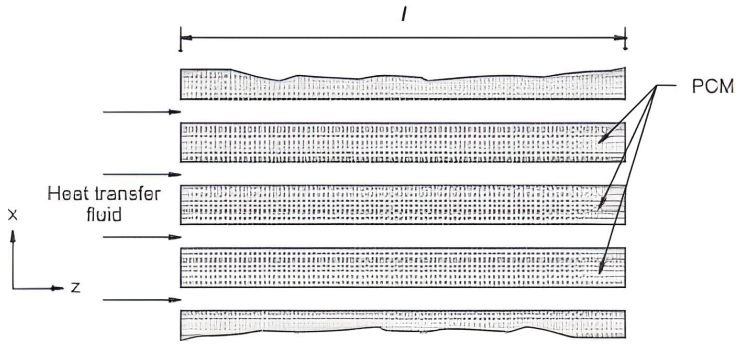

Figure 2.1: Slab LTES

- Shell and Tube LTES.

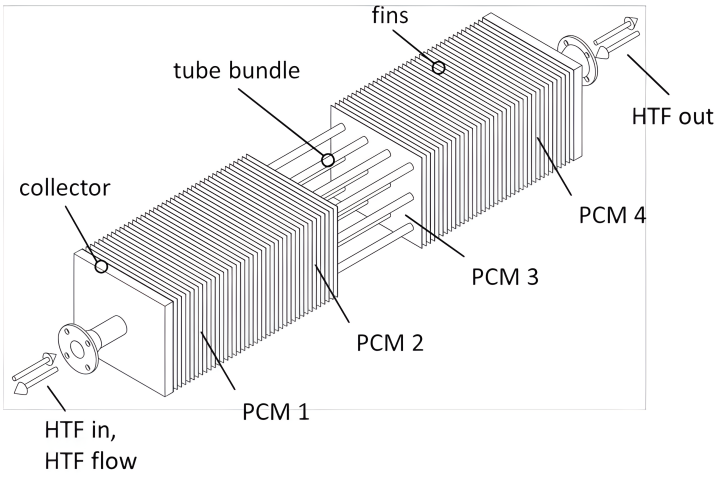

Figure 2.2: Shell and tube LTES

- Cylindrical LETS.

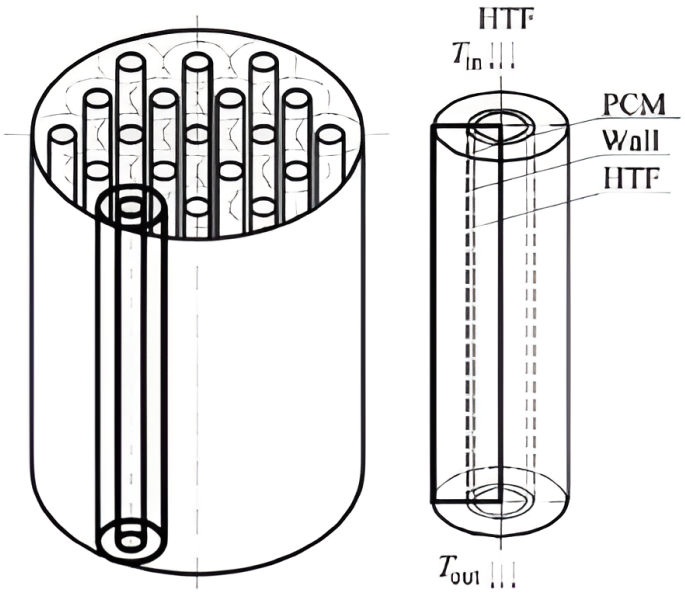

Figure 2.3: Cylindrical LTES

- Spherical LETS.

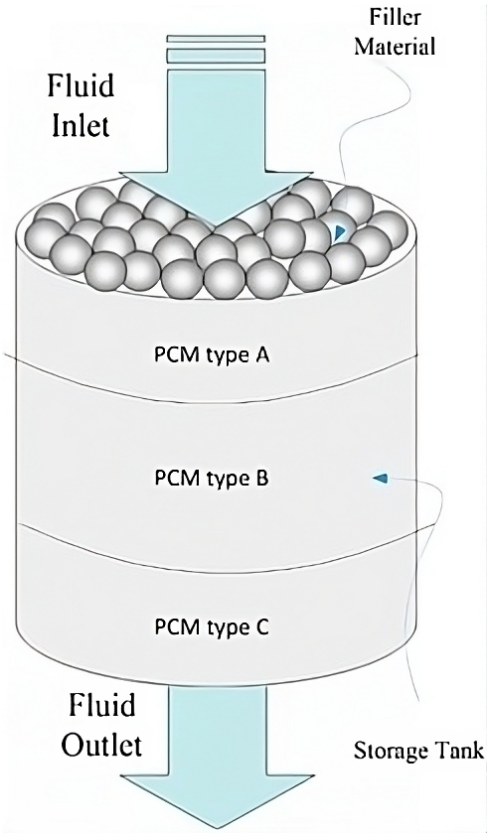

Figure 2.4: Spherical LTES

By following the previous logic, the spherical design is by far the most efficient one. However, for the purpose of this thesis, which is to define guidelines for modelling LTES in object oriented programs, the slab design will be analyzed. The conclusions can be extended to other configurations as well.

2.1. Phase Change Physics

When Modelling a slab of PCM, the internal heat transfer, when heat is provided, represents the critical aspect. When the material is in the solid state, and heat is provided to it, the heat transfer mode is conduction. However, when the material reaches its melting temperature, phase transitions occurs and liquid and solid states coexist until the PCM is fully melted. From solid to liquid state, the main heat transfer mode changes from conduction to convection. Furthermore, along the solid-liquid interface, the heat transfer is enhanced by the presence of motion in the liquid fraction of the PCM that is already melted. This motions derive by the change in the density of the PCM when it changes phase.

Overall, the physics behind the heat transfer in a PCM is described by the following

system of equations:

$$\begin{cases} \frac{\partial \rho}{\partial t} + \nabla \cdot \rho \vec{V} = 0 \\ \frac{\partial u}{\partial t} + u\frac{\partial u}{\partial x} + v\frac{\partial u}{\partial y} = \frac{1}{\rho}\left[-\frac{\partial p}{\partial x} + \mu\left(\frac{\partial^2 u}{\partial x^2} + \frac{\partial^2 u}{\partial y^2}\right) - A(T)u\right] \\ \frac{\partial v}{\partial t} + u\frac{\partial v}{\partial x} + v\frac{\partial v}{\partial y} = \frac{1}{\rho}\left[-\frac{\partial p}{\partial y} + \mu\left(\frac{\partial^2 v}{\partial x^2} + \frac{\partial^2 v}{\partial y^2}\right) + g\rho\beta\left(T - T_m\right) - A(T)v\right] \\ \frac{\partial T}{\partial t} + u\frac{\partial T}{\partial x} + v\frac{\partial T}{\partial y} = \frac{k}{\rho c_P}\left[\frac{\partial^2 T}{\partial x^2} + \frac{\partial^2 T}{\partial y^2}\right] \end{cases} \tag{2.1}$$

In the above system, the first is the continuity equation, the second and the third are the momentum equations respectively in the x and y direction (where x is the parallel to the ground and y is the perpendicular) and the fourth is the energy equation. ρ is the density of the material, u and v are the velocities of the material in the x and y axis respectively, p is the pressure, μ is the dynamic viscosity, g is the acceleration due to gravity, β is the thermal expansion coefficient, T_m is the melting temperature, k is the thermal conductivity, c_P is the specific heat capacity and $A(T)$ is a source term used to model the flow of the PCM during the phase change noted as the Kozeny-Carman parameter, defined as:

$$A(T) = \frac{C\left(1 - B(T)\right)^2}{\left(\phi(T)^3 + q\right)} \tag{2.2}$$

where C and q are arbitrary constants of values 10^5 and 10^{-3} respectively. $\phi(T)$ is the melt fraction of the PCM, and it is a function of temperature.
To properly study heat transfer under phase change, all equations in system 2.1 must be solved. It is a very complex system of partial differential equations and the solution is unsteady due to the movement of the solid-liquid interface in time.
In the following sections, different modelling approaches for the internal heat transfer of the PCM slab are presented as well as their strengths, limitations and assumptions.

2.1.1. Single Slab Lumped System Modelling

When modelling a physical system, the simplest way should always be analyzed to see if it is acceptable, so to avoid making the problem too complicated and computationally intensive. When heat is provided to a PCM slab, the easiest way to model it is to consider it as a lumped system. This approach can be verified through the Biot assumption. The assumption states that, when a body is subjected to convective heat transfer, it can be modelled as a single node under the condition that the Biot number is below 0.1. The Biot number is defined as follows:

$$Bi = \frac{hL_C}{k} = \frac{hV}{Ak} \tag{2.3}$$

where h is the convective heat transfer coefficient of the HTF, V is the volume of the PCM, A is the exchange area between the PCM and the HTF and k is the thermal conductivity of the PCM. $L_C = \frac{V}{A}$ is noted as the characteristic length for Biot assumption. A lumped system analysis is carried to verify the assumption for the case of a single PCM slab. For the analysis in question, typical values for the thermal conductivity of a PCM are considered. This makes sense since, as previously discussed, the thermal conductivity of PCMs is extremely low. Based on this assumption, the analysis is carried by changing the values of the characteristic length and convective heat transfer coefficient, and verify whether they are acceptable or not.
In the first case, the thermal conductivity of the PCM is selected to $3\,\frac{W}{mK}$ and the convective heat transfer coefficient is changed in a range from $600\,\frac{W}{m^2K}$ to $1\frac{W}{m^2K}$. The results are reported in Fig 2.5 It is evident that for realistic values of h, which could be easily reached with common fluids such as water, the characteristic length for the Biot assumption L_C is extremely low, which translates in a very high exchange area between the PCM and the HTF. At the same time, for more reasonable values of L_C, the h needed to respect the Biot assumption is reduced to very unrealistic values.

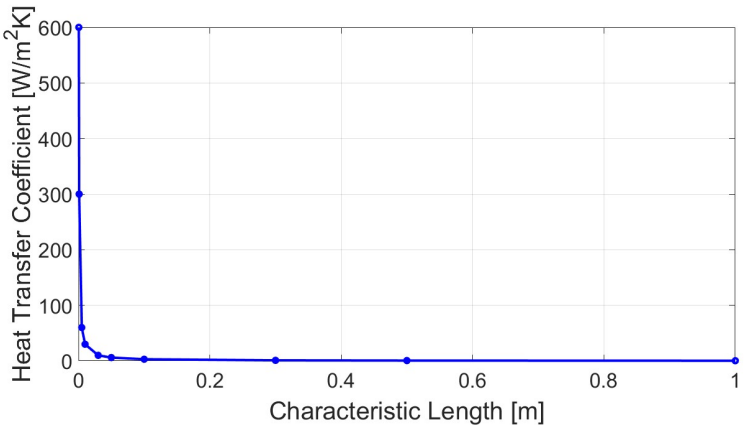

Figure 2.5: Biot analysis: h vs L_C

In the second case, the characteristic length is set to $0.005\,m$ and the thermal conductivity is changed in a range from $0.1\,\frac{W}{mK}$ to $1\,\frac{W}{mK}$. The results are reported in Fig 2.6 It is possible to notice that for typical values of PCM thermal conductivity, the convective heat transfer coefficient needed for the Biot assumption is extremely low.
The results from the Biot analysis are sufficient to state that modelling a PCM slab as a concentrated parameter is a wrong approach. The reason can be found once again in the extremely low thermal conductivity of the materials that are employed. From a physical point of view, when subjected to external heat transfer, the internal temperature gradient of the PCM slab cannot be neglected, i.e. considering that the entirety of the slab is at

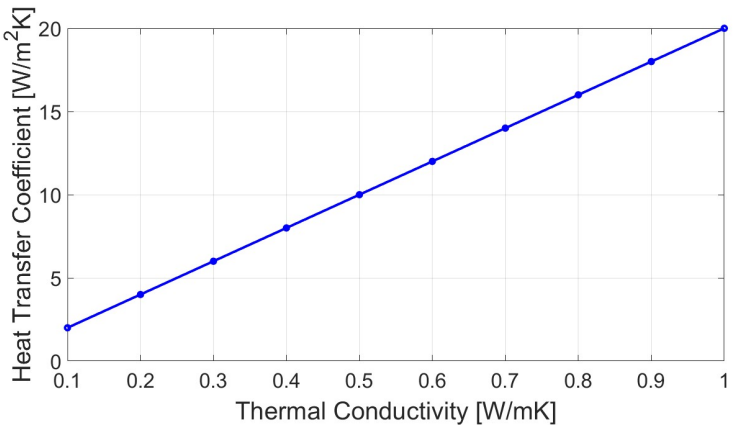

Figure 2.6: Biot analysis: h vs k

the same temperature is a wrong assumption.

2.1.2. PCM Domain Discretization

From the Biot analysis, it has been established the need to discretize the domain in order to account for the temperature gradient in the slab. In Fig 2.7, the geometry of the slab is presented.

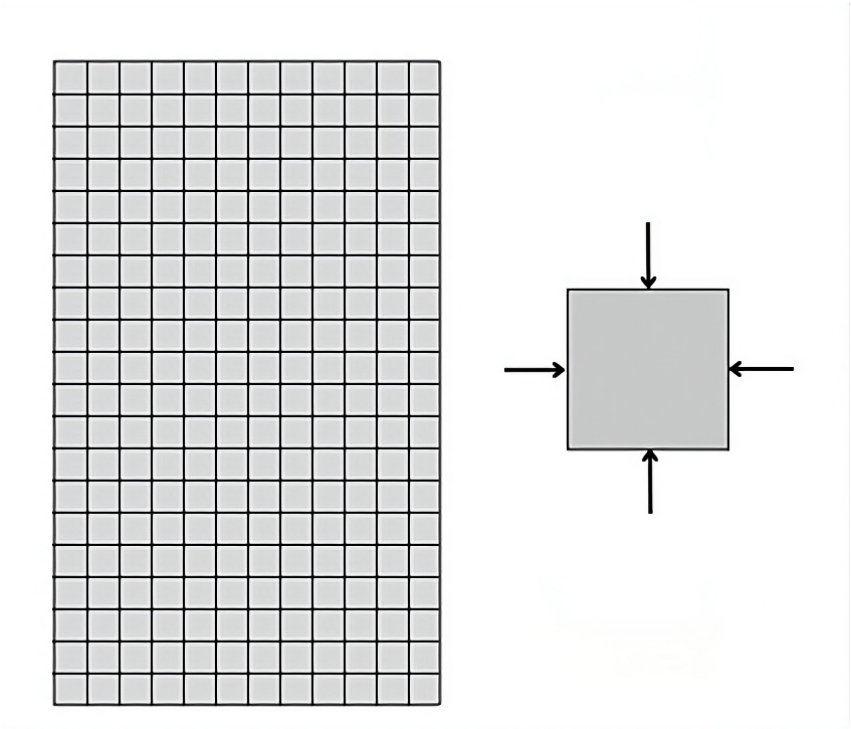

Figure 2.7: Slab discretization

It is assumed that the temperature gradient inside the slab develops only in the x and

y directions. This assumption is plausible if it is considered that the dimension in the z direction is high enough to not create boundary effects on the edges. With this assumption, the discretization of the domain becomes 2D.

The discretization is then employed to solve the energy equation from the system 2.1. In the model, the following assumptions are considered:

- Natural convection during phase change is neglected.
- Heat transfer along the z direction is not considered.
- Conduction is considered as the only way of heat transfer.
- Buoyancy forces due to density change are neglected.

As shown in Fig 2.8, depending on the number of vertical and horizontal nodes, the slab is divided in cells with the following dimensions:

$$\Delta x = \frac{L}{N-1} \tag{2.4}$$

$$\Delta y = \frac{H}{M-1} \tag{2.5}$$

where L is the thickness of the slab, H is the height, N is the number of horizontal nodes and M is the number of vertical nodes.
The energy equation is solved with a finite difference scheme as follows:

$$\rho c_P \frac{dT}{dt} = k\left(\frac{T\left(i,j+1\right)+T\left(i,j-1\right)-2T\left(i,j\right)}{\Delta x^2}+\frac{T\left(i+1,j\right)+T\left(i-1,j\right)-2T\left(i,j\right)}{\Delta y^2}\right) \tag{2.6}$$

The finite difference method allows to monitor the temperature evolution in different zones of the slab as a function of time. However, the properties of the material change depending on the temperature. For this reason, it is required to model the variability of the thermodynamic properties of the PCM with temperature.

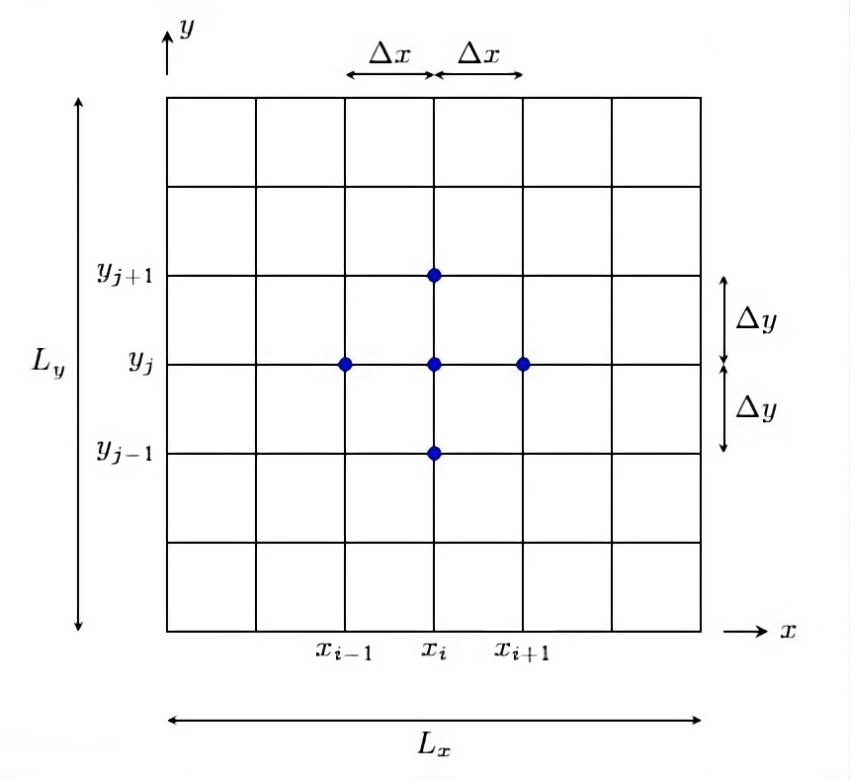

Figure 2.8: 2D grid

2.1.3. PCM Properties Variability with Temperature

Due to the phase transition, the density, thermal conductivity and specific heat capacity of the PCM change with temperature. To properly model the heat transfer with phase change, it is mandatory to implement relationships that consider their variability. In Fig 2.9 - 2.11, the specific heat capacity, density and thermal conductivity of a PCM are visualized for a typical charging process of the slab.

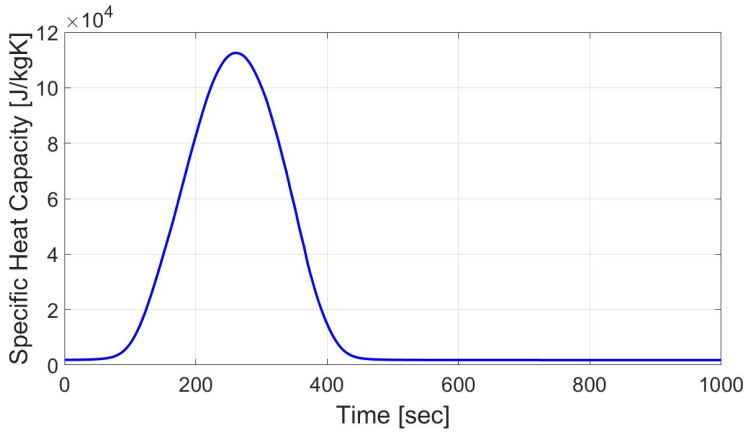

Figure 2.9: PCM specific heat capacity

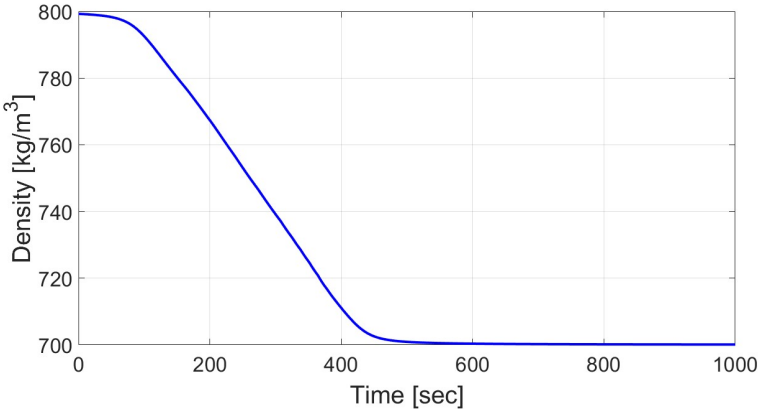

Figure 2.10: PCM density

When the material is either in the solid or liquid state, the thermodynamic properties are well defined. During the phase change, the properties can be calculated by employing a non dimensional parameter dependent on the temperature, called melt fraction. The melt fraction is defined as follows:

$$\phi(T) = \frac{T - \left(T_m - \frac{\Delta T}{2}\right)}{\Delta T} \tag{2.7}$$

where T_m is the melting temperature of the PCM and ΔT is the temperature range of phase transition.

For the definition of the properties during phase change, experimental correlations from literature have been employed. In particular, Halimov et al. [34] developed continuous functions for the specific heat capacity, density and thermal conductivity with tempera-

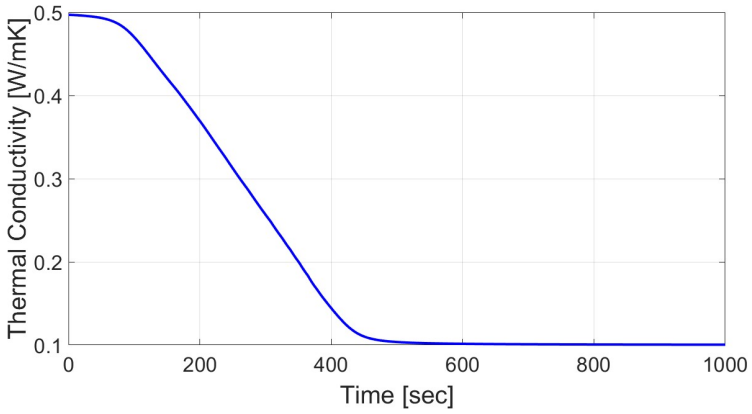

Figure 2.11: PCM thermal conductivity

ture. The relations are here reported:

$$\rho\left(T\right) = \rho_S\left(1-\phi\left(T\right)\right) + \rho_L\phi\left(T\right) \tag{2.8}$$

$$k\left(T\right) = k_S\left(1-\phi\left(T\right)\right) + k_L\phi\left(T\right) \tag{2.9}$$

$$c\left(T\right) = c_{0,S}\left(1-\phi\left(T\right)\right) + c_{0,L}\phi\left(T\right) + \Delta H_m \frac{\frac{2}{\Delta T}}{\pi\left[\left(\left(T-T_m\right)\left(\frac{2}{\Delta T}\right)\right)^2+1\right]} \tag{2.10}$$

where ρ_S is the density in the solid state, ρ_L is the density in the liquid state, k_S is the thermal conductivity in the solid state, k_L is the thermal conductivity in the liquid state, $c_{0,S}$ is the specific heat in the solid state, $c_{0,L}$ is the specific heat capacity in the liquid state and ΔH_m is the enthalpy change of phase transition. The specific heat capacity during phase change is defined as a baseline contribution that weights the solid and the liquid specific heats based on the melt fraction and a contribution given by the latent heat of fusion.

The Modelica model takes as inputs the properties of the PCM in the solid and liquid states, the initial temperature and boundary conditions of the slab, the dimensions of the slab and the number of vertical and horizontal nodes. Based on the inputs, the slab spatial domain is discretized and initialized, and the energy equation is solved for each node. Based on the temperature of the nodes, the thermodynamic properties are consequently calculated based on the equations previously presented.

2.1.4. Initial and Boundary Conditions

The initial and boundary conditions must be specified for the solution of the problem. The initial conditions are represented by the initial temperature of the PCM. In the model, for the initialization process, it is assumed that the slab is all at the same temperature. Based on the initial condition, melting or solidification process is defined:

$$\begin{cases} T > T_m & solidification \;\; process \\ T < T_m & melting \;\; process \end{cases} \tag{2.11}$$

The boundary conditions indicate how the energy conservation equation is solved at the edges of the slab. In particular, the slab exchanges heat with the HTF along its verticcal edges, meanwhile along the horizontal ones no interaction occurs. This is translated in Dirichlet conditions on the horizontal edges and Neumann conditions on the vertical ones. The heat equation is then consequently solved at the edges:

$$\begin{cases} T = T_{fixed} & horizontal \;\; edges \\ \rho c \left(W dy\right) \frac{dT}{dt} = \frac{Q}{dx} - k \left(T\left(1\right) - T\left(2\right)\right) & vertical \;\; edges \end{cases} \tag{2.12}$$

where W is the dimension of the slab in the z direction, dy is the height of the cell, Q is the heat that is exchanged between the HTF and the PCM, dx is the thickness of the cell, $T\left(1\right)$ is the temperature of the boundary cell and $T\left(2\right)$ is the temperature of the neighbouring cell. The energy conservation equation is solved in the same way for the opposite side of the slab by substituting $T\left(1\right)$ with $T\left(N\right)$ and $T\left(2\right)$ with $T\left(N-1\right)$.

2.2. Model Assumptions Validation

In this section, the assumptions that have been made in the model for the internal heat transfer in the slab are verified. Since the enthalpy approach that is adopted in the finite difference model does not account for internal motion of the material during the phase change, CFD simulations have been employed to compare the results. The simulations have been carried in Ansys Fluent.

The section is divided as follows: the specifications for the setup in Ansys Fluent for the CFD simulations are presented, heat transfer problem is solved with CFD with and without the resolution of the flow equation and results are compared by changing the dimensions of the slab. Finally, the results are compared with the ones from the Modelica model and an empirical correlation for the natural convection enhancement coefficient is

tested from literature.

2.2.1. CFD Setup Specifications

The software employed for the CFD simulations is Ansys Fluent. Ansys Fluent is a widely used computational fluid dynamics software. It is used for simulating and analyzing fluid flow, heat transfer, chemical reactions, and other related phenomena in various engineering and scientific fields.
For the simulations, the mesh applied to solve the slab heat transfer problem is a structured grid, as shown in Fig 2.12.

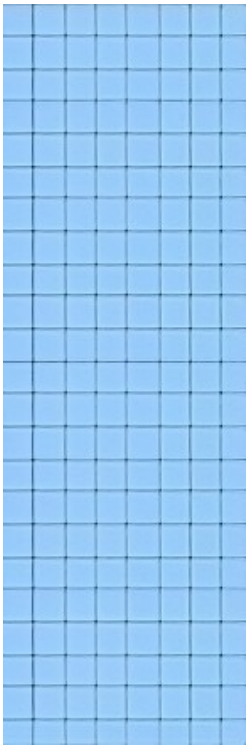

Figure 2.12: Mesh

The execution is parallel and the number of processing units is set to two. The acceleration due to gravity is activated to account for the buoyancy term during the phase transition. The problem is solved as transient. The fluid is considered to be laminar due to the very low velocities reached in the problem, and the "Solidification and Melting" model provided by Ansys Fluent is employed for the resolution of the phase change. Furthermore, the solution methods use a SIMPLE scheme for the pressure-velocity coupling and for the spatial discretization a second order for pressure and a second order upwind for momentum and energy. The residuals are set to 10^{-6} for continuity, x-velocity and y-velocity and 10^{-9} for energy.

2.2.2. Slab Dimensions Impact on CFD Results

Ansys Fluent allows to solve the heat transfer with phase change by solving either both the energy equation and the flow equation and only the energy equation. It is important to notice that the case with only the energy equation solves the problem in the exact way that is implemented in the Modelica model.
The impact of the slab dimensions is measured in two ways. In the first one, the thickness of the slab is fixed and the height is changed, while in the second the height is fixed and the thickness is changed. For each configuration, the problem is solved in Ansys Fluent by employing only the energy equation and both energy and flow equations, which is considered to be the true case, and results are compared.
The dimension of the slab is measured through an adimensional parameter called aspect ratio, defined as follows:

$$AR = \frac{Height\ of\ the\ slab}{Thickness\ of\ the\ slab} \tag{2.13}$$

The comparison is made by measuring the deviation of the melting times for the two solution methods.

Slab Height Impact

For this case, the thickness of the slab is fixed to 2 cm and the height is changed to estimate the effect of natural convection. In Fig 2.13 the results are reported.

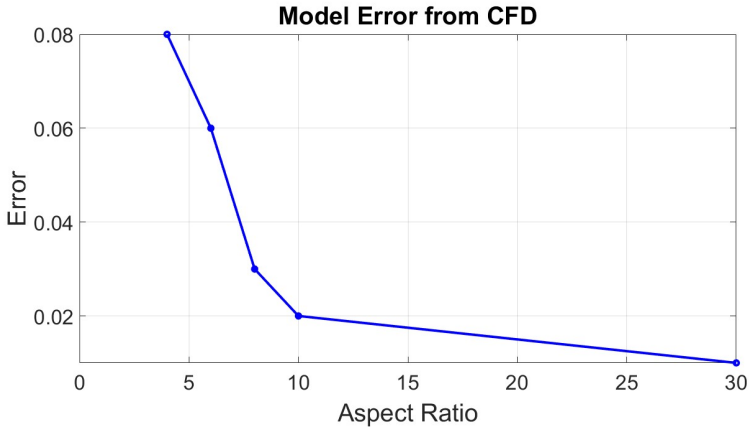

Figure 2.13: Error from CFD: variable height impact

In the graph, the error from the true case for each aspect ratio is reported. It is possible to notice that, by decreasing the height of the slab, which means decreasing the aspect ratio, the error increases but it never reaches high values. This is an indication that the intensity of natural convection is not very sensitive to the height of the slab.

The reason that the decrease of the aspect ratio leads to a higher impact of natural convection can be explained by an increase of the specific surface of the solid-liquid interface with respect of the slab volume.
The thinner the slab, the lower the specific surface on which the heat transfer can be enhanced through natural convection created by the motion of the liquid PCM.
In Fig 2.14 it is possible to visualize the difference of the two solution methods for thin slabs.

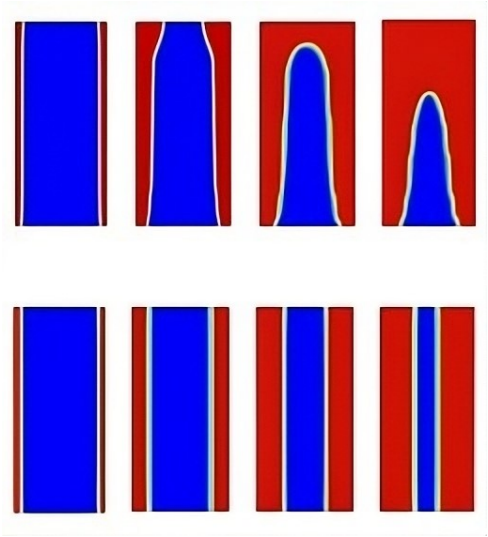

Figure 2.14: Contours of melt fraction

Empirical Correlation for Natural Convection Enhancement

Vogel et al. [35] developed a relation for a thermal conduction enhancement coefficient for a PCM flat plate. The relation takes into account the intensity of natural convection through the Rayleigh number and the geometrical aspect through the aspect ratio. The relation is defined as follows:

$$\begin{cases} \epsilon = 1 & Ra^{\frac{1}{6}} \left(AR\right)^{-\frac{1}{4}} < 2.73 \\ \epsilon = 0.57 \left(Ra^{\frac{1}{6}} \left(AR\right)^{-\frac{1}{4}}\right) - 0.38 & Ra^{\frac{1}{6}} \left(AR\right)^{-\frac{1}{4}} > 2.73 \end{cases} \tag{2.14}$$

where AR is the aspect ratio and is defined as previously stated and Ra is the Rayleigh number, which is calculated as follows:

$$Ra = \frac{g\beta \left(T_{wall} - T_m\right) L^3}{\nu\alpha} \tag{2.15}$$

where β is the thermal diffusivity of the PCM in the liquid state, T_{wall} is the temperature on the vertical boundaries of the slab, T_m is the melting temperature of the PCM, L is the thickness of the slab, ν is the kinematic viscosity of the PCM in the liquid state and α is the thermal diffusivity.
The relationship has been implemented in the Modelica model and tested against CFD results to verify its validity and limit.

Comparison of Modelica Model and CFD: Slab Height

The model implemented in Modelica is now compared with the results from CFD. For each aspect ratio, the model is run firstly considering only conduction as the heat transfer mode, and secondly by employing the relationship for the thermal conductivity enhancement coefficient developed by Vogel et al. In Figure 2.15 the results are reported. In the graph it is possible to notice the melting time error with respect to the true case.
Two observations are relevant: firstly, for the conductive case the error trend is almost the same as the one in Fig 2.13 that was solved through CFD, meaning that the finite difference method solves the energy equation correctly. Secondly, the model that considers the natural convection enhancement coefficient presents a much more stable error. The relationship is able to properly evaluate the effect of natural convection created by changing the height of the slab.

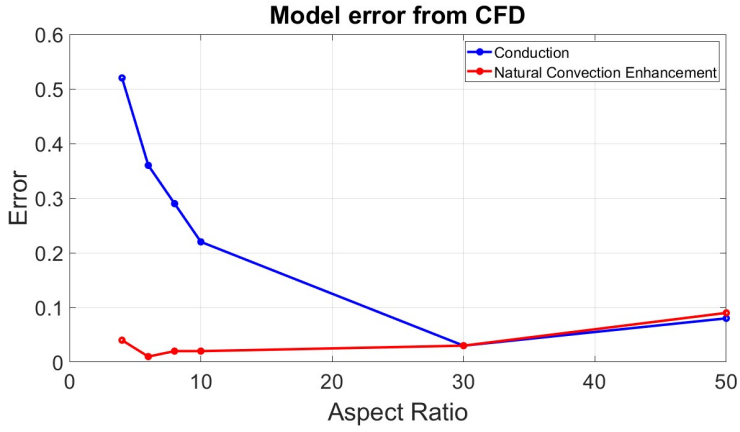

Figure 2.15: Error from CFD: conduction and empirical correlation

Since the results show that the model with the empirical correlation is more accurate, the discussion will take it as a reference from now on.

An additional validation is conducted to verify if the model implemented in Modelica is also able to accurately replicate the temperature profile, beyond correctly estimating the melting time. For each of the simulations, the temperature difference at a specific time

after the PCM is completely melted is calculated. The results are reported in Fig 2.16 It is possible to observe that the model is very accurate, since the error never overcomes the value of 2%.

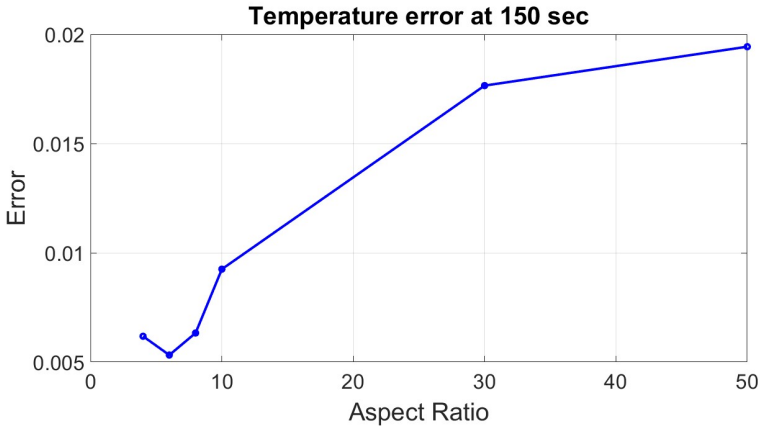

Figure 2.16: : Temperature error from CFD

Overall, the model that considers the enhancement of thermal conductivity is more precise, and the accuracy increases the lower the aspect ratio. This indicates that the more convection becomes important in the heat transfer mechanism, the lower the error with respect to CFD, because the deviation due to the only conductive case is reduced.

Comparison of Modelica Model and CFD: Slab Thickness

A comparison between the Modelica model and CFD is carried when increasing the thickness of the slab. The height is considered to be constant and fixed at 30 cm. In Fig 2.17, the results are reported.

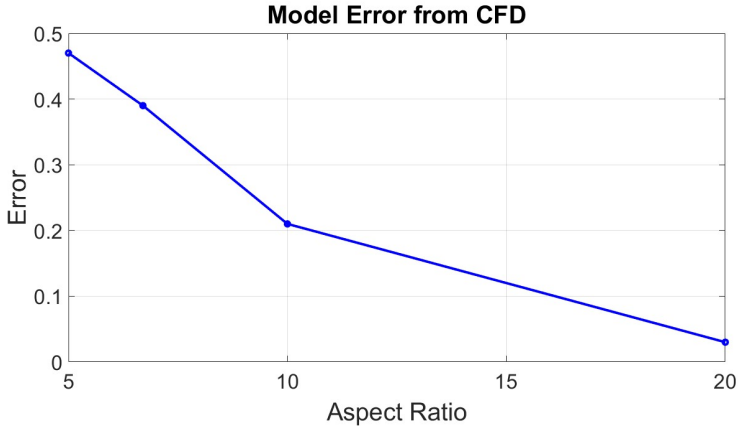

Figure 2.17: Error from CFD: variable thickness

When a square cavity is subjected to heat from any of its sides, the dimension that in-

creases the natural convection effect is the one that is perpendicular to the edge to which heat is applied. For this reason, in the slab case, the thickness should have a much bigger effect on the heat transfer than the height. Clearly, natural convection has a way bigger impact, but the most important observation to make is that the empirical correlation from Vogel et al. is not able to properly define the enhancement coefficient. In particular, the lower the aspect ratio, the higher the error, which reaches values of almost 50%. Such a deviation is not acceptable for a generic model, and must be overcome.

2.2.3. Fictive Thermal Conductivity Model

CFD simulations are now employed to develop a thermal conductivity enhancement coefficient that is to be applied during phase change. Specifically, different simulations are run by changing the thickness of the slab. Subsequently, the enthalpy of the central node of the mesh is determined for both the conductive and convective solution. The enhancement coefficient is calculated as follows:

$$\epsilon = \frac{H_{convection}}{H_{conduction}} \tag{2.16}$$

The enhancement coefficient is determined as the ratio of the energy of the node when natural convection is considered in the heat transfer and when only conduction is considered. In the finite different scheme, the coefficient multiplies the thermal conductivity of the material when the temperature is in the phase change range. This allows to create a fictive thermal conductivity that accounts for the heat transfer enhancement due to the motion of the melted PCM.
Since in both cases the slab reaches the same final temperature, the final enthalpy of the node is the same. This would make the ratio equal to 1. For this reason, the enthalpy content is evaluated as the sum of the enthalpy at each time step of the simulation, until the slab reaches the final temperature:

$$\epsilon = \frac{\sum_{i=1}^{t} h_{i,convection}}{\sum_{i=1}^{t} h_{i,conduction}} \tag{2.17}$$

where t is the simulation time that is needed to reach the same temperature for both solution methods and h_i is the enthalpy of the node at the i_{th} time step.
For each value of thickness, the resulting enhancement coefficient is applied to the Modelica model, and results are compared. The thickness of the slab is spanned in a range of values from 1 cm to 4 cm. The reason for it is that, from literature, it doesn't result that slabs used for latent thermal energy storage have higher thicknesses.

In Fig 2.18 - 2.19, it is reported the case for a 2 cm thick slab. Fig 2.18 reports the conductive and convective temperatures as a function of time from CFD, while Fig 2.19 reports the same from Modelica.

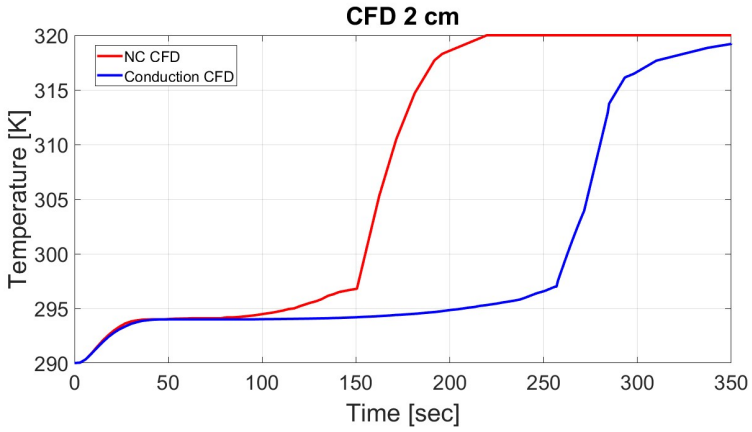

Figure 2.18: CFD temperature as a function of time

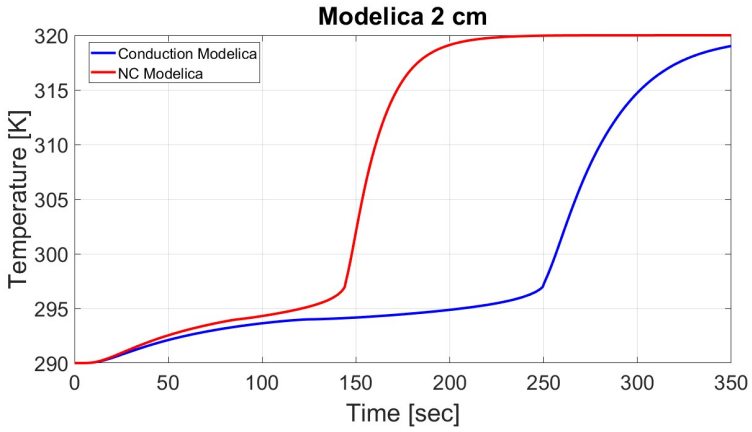

Figure 2.19: Modelica temperature as a function of time

The results from the simulations are reported in the scatter plot in Fig 2.20. To define the correlation between the enhancement coefficient and the Rayleigh number, the data are interpolated with an exponential function and the correspondent equation is to be considered the ϵ-Ra relation. In Fig 2.21, it is possible to visualize the relation between the enhancement coefficient and the Rayleigh number.

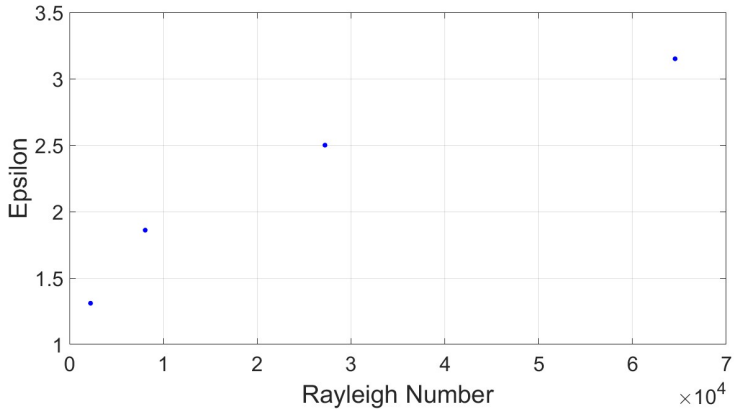

Figure 2.20: Enhancement coefficient dependence on natural convection

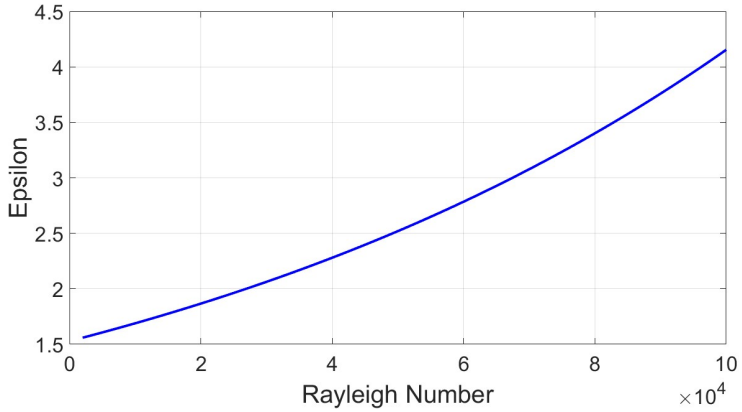

Figure 2.21: ϵ - Ra relation

2.2.4. Mesh Independence Analysis

Since the validation of the model has been carried out by comparing the results with the ones coming from CFD simulations, it is imperative to conduct a mesh independence

analysis to check whether the results from CFD can be trusted to be correct.
A mesh independence analysis is conducted by changing the mesh type and the resolution of the mesh, and comparing for each simulation the same parameter under the same boundary and initial conditions. The better is the mesh, the closer the value of the parameter is to the true one. Then, the final mesh is selected based on the accuracy of the results that is needed to be achieved and the computational cost.
For the slab, the mesh type is a structured grid. Consequently, the mesh independence analysis is conducted just by changing the cell size. The smaller the cell, the more precise the results. The parameter that has been chosen to be compared is the full melting time of the slab.
The analysis has been conducted for the case of a slab of dimensions $0.3\,x\,0.02\,m$. The cell sizes that have been considered are 0.002, 0.001, 0.0005, 0.00025 and $0.000125m$. This results in the following number of cells:

Cell size [m]	Number of cells
0.002	1500
0.001	6000
0.0005	24000
0.00025	96000
0.000125	384000

Table 2.1: Mesh number of cells

From Fig 2.22, it is possible to see the outcome of the analysis. As expected, the higher the number of cells, the longer it takes for the slab to completely melt. In the graph it is reported the non dimensional time for melting, defined as follows:

$$t_{adimensional}\,(i) = \frac{t_{melting}\,(i)}{t_{max,simulation}} \tag{2.18}$$

where $t_{melting}\,(i)$ is the time that the PCM takes to melt in simulation i-th, and $t_{max,simulation}$ is the time that the PCM takes to melt for the simulation with the highest number of cells.
The results of the analysis show that by choosing smaller cells, the solution converges to the true value. However, the results do not deviate too much from each others. For this reason, the simulations have been run with cells of size $0.0005\,m$.

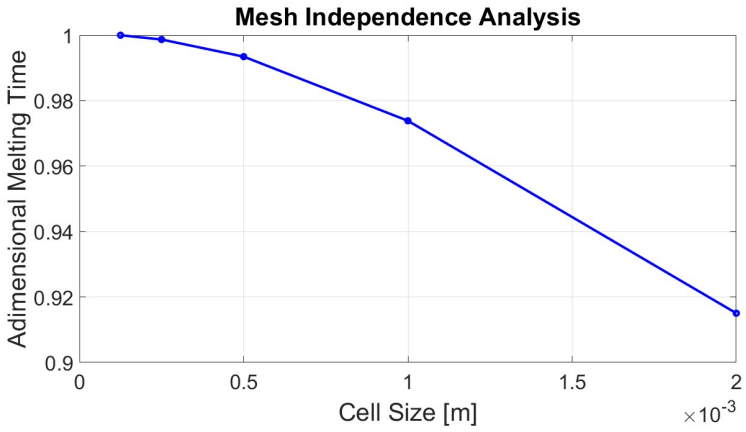

Figure 2.22: Mesh independence analysis

2.2.5. Final Internal PCM Heat Transfer Model

The final model for the internal PCM heat transfer is completed by combining the results obtained from the previous analysis. In the final model, the heat equation is solved through the finite difference scheme, and the fictive thermal conductivity of the PCM during phase change is calculated either with the empirical correlation from literature or the ϵ-Ra correlation developed through CFD analysis.
The choice between the two methods depends on the geometry of the slab. In particular, from Fig 2.15, it is observed that when the aspect ratio reaches values below 10, the error starts to become non negligible. Furthermore, from Fig 2.17, when the aspect ratio is lower than 10, the error starts increasing more rapidly. From these observations, the following conclusions are reached:

$$\epsilon = \begin{cases} 0.57\left(Ra^{\frac{1}{6}}\,(AR)^{-\frac{1}{4}}\right) - 0.38 & AR > 10 \\ \epsilon = 1.528e^{1E-05Ra} & AR > 10 \end{cases} \tag{2.19}$$

3 | Heat Interaction between HTF and PCM

This chapter focuses on the heat interaction between the heat transfer fluid (HTF) and the PCM slabs. To model the heat interaction between the fluid and the material, a fluid-dynamic analysis of the flow in the channel has to be conducted. Furthermore, due to the phase change of the PCM and hence the presence of liquid, containment has to be considered as well in the model. This makes the heat interaction even more challenging. The chapter is organized as follows: firstly, a fluid-dynamic analysis of the flow in the channels is presented, and boundary and initial conditions of the model are discussed. Subsequently, a boundary layer analysis inside the channel is conducted. Finally the thermal resistance model for the containment of the PCM is presented.

3.0.1. Channel Geometry

In a slab LTES, the HTF flows in the spacing between the PCM slabs. The fluid then exchanges heat with each of the slabs that create the channel. The flow channel geometry is represented in Fig 3.1.

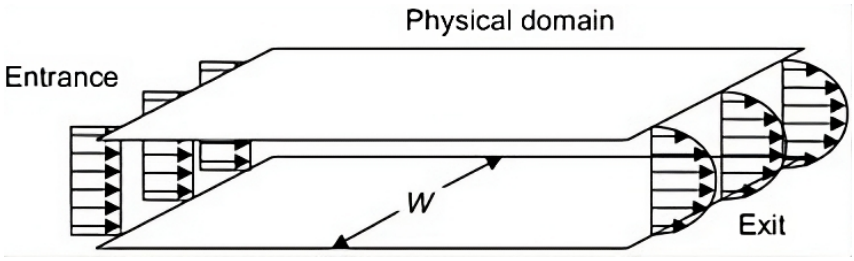

Figure 3.1: : Flow channel between slabs

In the storage, the number of flow channels is correlated to the number of slabs that are present. If in the storage there are N slabs, then there are $N-1$ flow channels. This happens because it is considered that the two extreme slabs are in contact with the HTF only on onse side, meanwhile the other is directly in contact with the storage

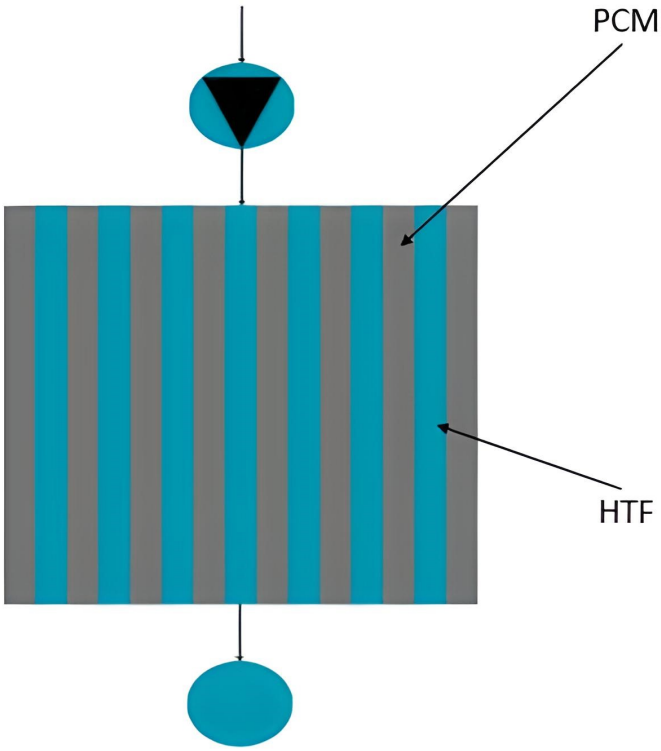

Figure 3.2: Slab LTES frontal view

encapsulation. In Fig 3.2, a frontal view of the storage is presented.
The fluid-dynamic analysis for the HTF flow in the channels is conducted considering the geometry that has been just presented.

3.0.2. Fluid-Dynamic Analysis of HTF Flow

The heat transferred between the HTF and the PCM is driven by the difference in temperature between the two. During the charging process, the HTF has a higher temperature than the PCM, which is at temperature below its melting point, while for the discharging process the HTF is at a lower temperature than the PCM, which is at a temperature above its melting one. This is summed up as follows:

$$\begin{cases} T_{HTF} > T_{PCM} \quad \wedge \quad T_{PCM} < T_m & charging \quad process \\ T_{HTF} < T_{PCM} \quad \wedge \quad T_{PCM} > T_m & discharging \quad process \end{cases} \tag{3.1}$$

where T_m is the melting temperature of the PCM.
The heat that is transferred between the HTF and the PCM is computed as follows:

$$Q = hS\left(T_{HTF} - T_{PCM}\right) \tag{3.2}$$

where h is the convective heat transfer coefficient of the HTF and S is the contact surface between the HTF and the PCM slab. The convective heat transfer coefficient is a function of the channel dimensions, velocity and thermodynamic properties of the fluid. In Fig 3.3, the geometry of the slab and its dimensions are reported.

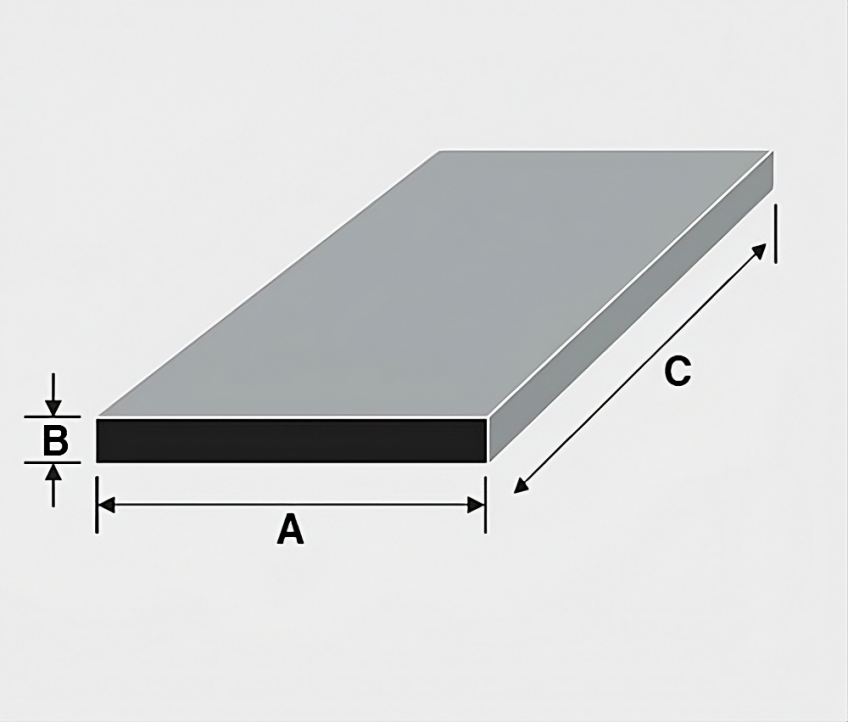

Figure 3.3: Slab geometry and dimensions

Following the notation in Fig 3.3, the exchange area is computed as:

$$S = AC \tag{3.3}$$

As previously stated, the convective heat transfer coefficient h depends on the fluid-dynamic state of the HTF flow in the channels. In Modelica, a model for the calculation of h has been implemented. The model takes as input the dimensions of the channel, the thermodynamic properties of the HTF (density, thermal conductivity, dynamic and kinematic viscosity, and specific heat capacity) and the mass flow rate of the HTF in the channel. The model subsequently calculates the velocity of the fluid and the Reynolds

number. The Reynolds number is then used to determine whether the flow is laminar or turbulent. Once the state of the flow is determined, the appropriate correlation is employed to determine the Nusselt number. Finally, the convective heat transfer coefficient is calculated.
It is important to clarify that the mass flow rate of HTF in the channel depends on the number of slabs in the storage and the total mass flow rate that flows in the system:

$$\dot{m}_{channel} = \frac{\dot{m}_{system}}{N-1} \tag{3.4}$$

where $\dot{m}_{system}$ is the total HTF mass flow rate in the system (e.g. the mass flow rate in the heat pump), and N is the number of PCM slabs, which means that $N-1$ is the number of flow channels in the storage.
For the flow on a flat plate, the critical Reynolds number Re_{cr} is considered to be $5 \cdot 10^5$. The following condition applies:

$$\begin{cases} Re > Re_{cr} = 5 \cdot 10^5 & turbulent flow \\ Re < Re_{cr} = 5 \cdot 10^5 & laminar flow \end{cases} \tag{3.5}$$

The velocity of the HTF is computed from the mass flow rate in the channel as follows:

$$u = \frac{\dot{m}_{channel}}{\rho A_{cross}} \tag{3.6}$$

where ρ is the density of the HTF, and A_{cross} is the cross section of the channel, which remains constant. Following the notation in Fig 3.3, the cross section is computed as:

$$A_{cross} = As \tag{3.7}$$

where s is the spacing between neighbouring slabs, hence the thickness of the channel.
From the HTF velocity, it is possible to calculate the Reynolds number:

$$Re = \frac{\rho u L}{\mu} = \frac{uL}{\nu} \tag{3.8}$$

where L is the length of the slab (C from Fig 3.3), μ is the dynamic viscosity of the fluid and ν is the kinematic viscosity of the fluid.
Depending on the value of the Reynolds number, the flow is either laminar or turbulent. Based on the fluid-dynamic state of the flow, the relation for the calculation of the Nusselt

number is chosen as follows:

$$\begin{cases} Nu = 0.664\, Re^{0.5} Pr^{1/3} & laminar \quad flow \\ Nu = 0.0296\, Re^{4/5} Pr^{1/3} & turbulent \quad flow \end{cases} \tag{3.9}$$

where Pr is the Prandtl number determined as:

$$Pr = \frac{\mu\, c_P}{k} \tag{3.10}$$

where c_P is the specific heat capacity of the fluid and k is the thermal conductivity. The relations from in 3.9 are the Nusselt correlations for forced convection over flat plate [37]. Finally, the Nusselt number is employed to calculate the convective heat transfer coefficient h that determines the heat transfer rate between HTF and PCM slab:

$$h = \frac{Nu\, k}{L} \tag{3.11}$$

The flowchart in Fig 3.4 reports the algorithm that the Modelica model follows to compute the convective heat transfer coefficient h.

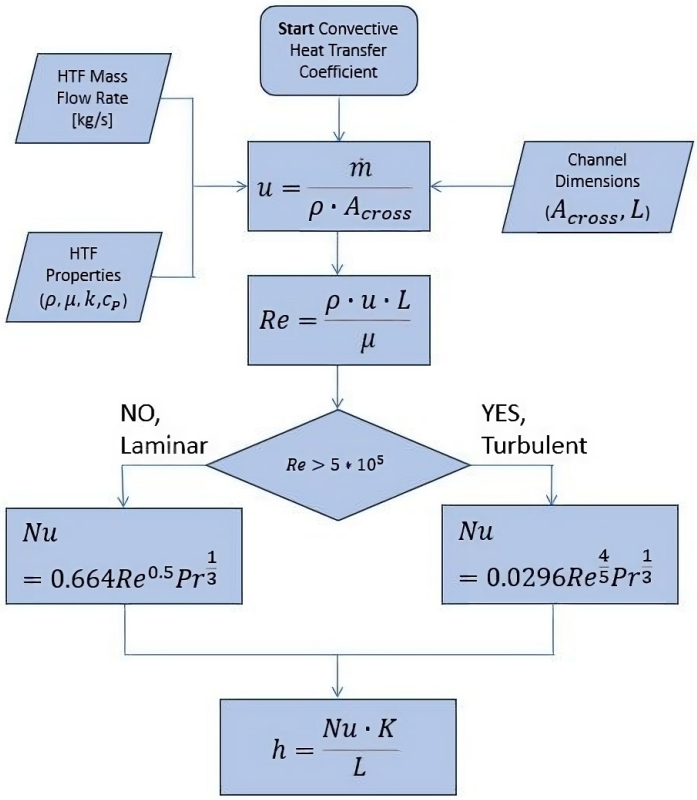

Figure 3.4: Flowchart: convective heat transfer coefficient

3.0.3. Boundary and Initial Conditions

When the LTES is integrated in wider systems, such as heat pumps, it is assumed that during and after the operation of the storage, the flow channels are filled with the HTF. When the storage is not used, the HTF and the PCM have the same temperature, i.e. they have reached the thermal equilibrium. This translates in the following initial conditions:

$$\begin{cases} T_{HTF} = T_{PCM} > T_m & discharging \;\; process \\ T_{HTF} = T_{PCM} < T_m & charging \;\; process \end{cases} \tag{3.12}$$

where T_m is the melting temperature of the PCM.
The initial conditions allow to take into account the fact that when the storage is operated, the HTF does not exchange heat with the PCM immediately at the desired temperature, but a transition time is needed for the working fluid to reach the operational temperature. When the HTF enters the channel at temperature T_∞ and the slabs are at a lower initial temperature T_s, a temperature boundary layer, also called thermal boundary layer, is created over the surface of the slab [38], as shown in Fig 3.5. The thermal boundary layer is associated with the temperature gradient near the surface of the slab.

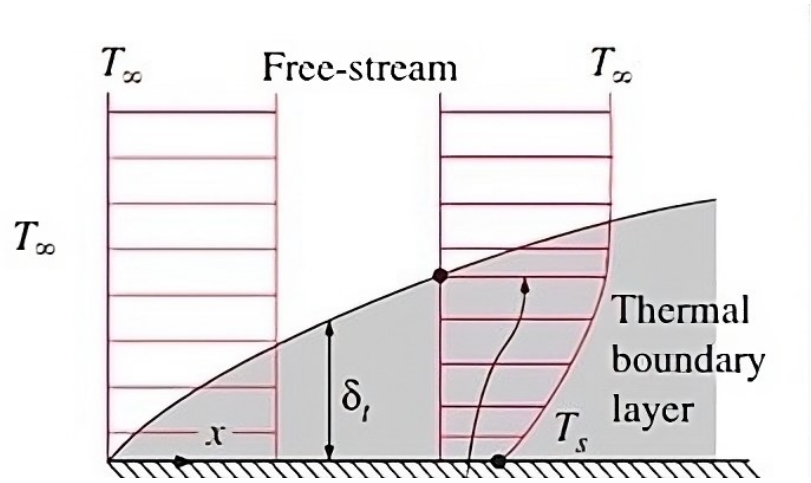

Figure 3.5: Thermal boundary layer

Initially, as the fluid approaches the flat plate, its temperature is nearly uniform, matching the free-stream temperature T_∞. As it flows along the surface of the plate, thermal gradients develop. The temperature of the fluid near the plate changes gradually. The thickness of the thermal boundary layer, denoted as δ_t, increases moving downstream along the plate. The temperature distribution within the thermal boundary layer typically follows a profile that varies from the plate surface to the free stream temperature.
In the model implemented in Modelica, the thermal boundary layer is not considered.

This translates in the following assumptions:

- The temperature gradient due to the thermal boundary layer is neglected.
- The HTF is assumed to be at the same temperature along the direction perpendicular to the flow.
- The properties of the HTF are determined at $T_{mean} = \frac{T_\infty + T_s}{2}$.
- The heat transferred between the HTF and the PCM is calculated considering T_∞ and the surface temperature of the slab T_s.

The model calculates the heat transfer as:

$$Q = hS\left(T_\infty - T_s\right) \tag{3.13}$$

3.0.4. Boundary Layer Analysis

When the HTF approaches the slab, its velocity is assumed to be nearly uniform and matches the free-stream velocity. However, as the fluid flows along the surface of the plate, it experiences frictional forces with the plate, which slow it down near the surface. This results in the development of a boundary layer where the velocity gradients are significant. The thickness of the velocity boundary layer, denoted as δ, increases moving downstream along the slab. Within the velocity boundary layer, the velocity of the fluid varies from zero at the plate's surface (no-slip condition) to the free-stream velocity away from the plate [39].
When a fluid passes between two slabs, the finite viscosity causes boundary layers to form on the inner surfaces of the upper and lower plates. The flow within these layers possesses non-zero vorticity, and is significantly affected by viscosity. On the other hand, the flow outside the layers is irrotational and essentially inviscid. This type of flow is usually termed potential flow. The thickness of the two boundary layers increases like $x^{1/2}$, where x represents distance, parallel to the flow, measured from the leading edges of the plates. It follows that, as x increases, the region of potential flow shrinks in size, and eventually disappears, as shown in Fig 3.6.
The two boundary layers develop until eventually they merge and interact with each other. The resulting merged boundary layer may exhibit different flow characteristics than the individual ones, such as altered velocity profiles and increased boundary layer thickness. The interaction between boundary layers may lead to increased friction between the fluid and the plates, which can result in higher energy dissipation and potentially higher pressure drop along the channel. It is, thus, important to verify if this condition occurs for

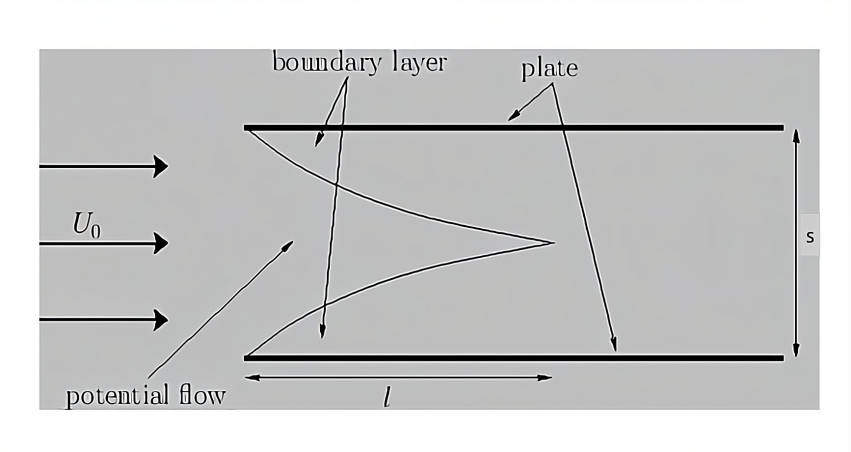

Figure 3.6: Velocity boundary layer between two slabs

the case under analysis.
In the model, an algorithm that calculates the thickness of the boundary layer that develops over the slab is implemented. The model is limited to verify if interaction occurs, but does not change the methodology for the fluid-dynamic analysis. The model calculates the thickness of the layer at the length of the slab, since δ is proportional to the flow coordinate x. To avoid interaction, the thickness of the boundary layer must be small with respect to half of the thickness of the channel:

$$\delta\left(L\right) << \frac{s}{2} \tag{3.14}$$

where L is the length of the slab and s is the thickness of the channel.
The model takes as input the Reynolds number calculated in equation 2.8, and based on whether the flow is laminar or turbulent applies the correct relation for the thickness of the boundary layer:

$$\begin{cases} \delta = 5\frac{L}{\sqrt{Re}} & laminar \quad flow \\ \\ \delta = 0.37\frac{L}{Re^{1/5}} & turbulent \quad flow \end{cases} \tag{3.15}$$

The thickness of the boundary layer behaves according to the Blasius solution conditions [36]. The turbulent boundary layer thickness formula, though, assumes that the flow is turbulent from the start of the boundary layer. This is not necessarily the case.
The flowchart in Fig 3.7 shows the algorithm coded in the model for the check of boundary layer interaction.

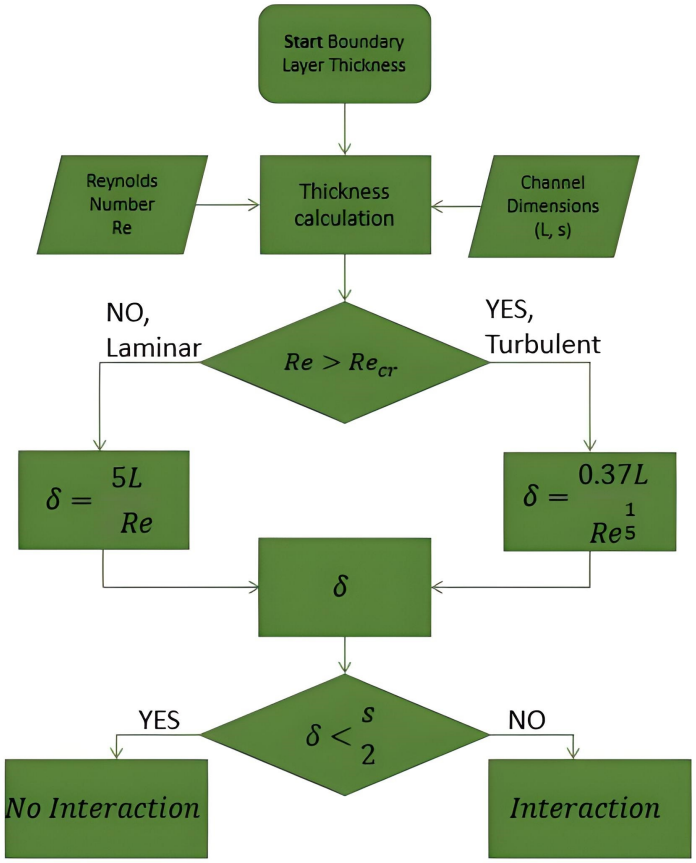

Figure 3.7: Flowchart: boundary layer interaction

Sensitivity analysis is conducted to analyze the impact of different parameters on the boundary layers. The purpose is to verify if, for the case in question, boundary layer interaction is likely to occur. For the test, a LTES with five slabs is considered. Overall, the results show that boundary layer interaction is unlikely to happen for the typical operation of the LTES in heat pump systems.

Mass Flow Rate

The impact of the HTF mass flow rate in the channel is tested for the interaction of the boundary layers. Realistic values of mass flow rate are considered starting from typical values of HTF flow rate in heat pump systems. The mass flow rate in the channels of the storage is calculated from the mass flow rate flowing in the heat pump. The results of the analysis are presented in Fig 3.8.

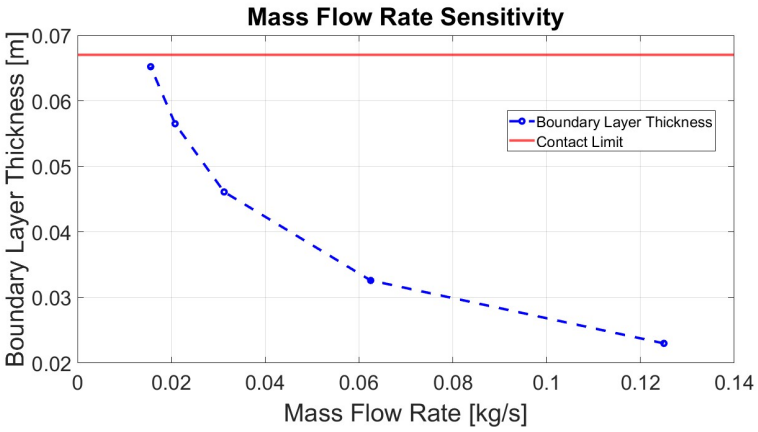

Figure 3.8: Boundary layer analysis: mass flow rate

In the graph, the contact limit is represented by half of the thickness of the channel. Since the thickness of the boundary layer is inversely proportional to the Reynolds number, the lower the mass flow rate in the channel the higher the risk of interaction. If the mass flow rate in the heat pump is kept constant, the results indicate that the higher the number of slabs in the storage the higher the risk of boundary layer interaction as well.

Slab Length

The impact of the length of the slab is tested for the interaction of the boundary layers. The results are reported in Fig 3.9.

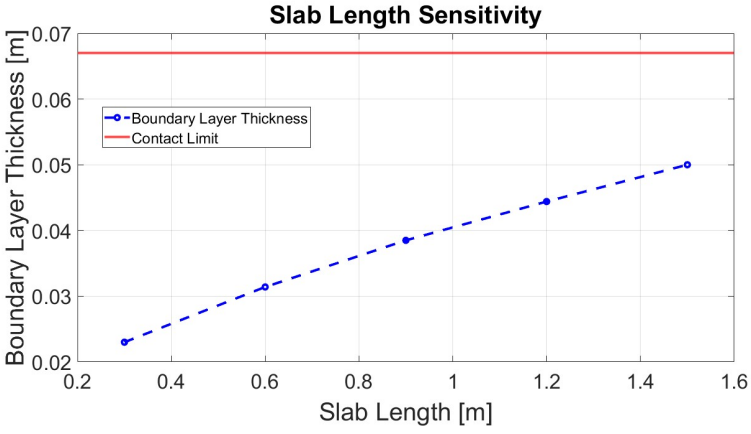

Figure 3.9: Boundary layer analysis: slab length

In the graph, the contact limit is represented by half of the thickness of the channel. Since the thickness of the boundary layer is directly proportional to the length of the channel, i.e. the length of the slab, the longer the slab the higher the risk of interaction. However, even for very long slabs, such as 1.5 m, the risk is low.

Channel Cross Section

The impact of the cross section of the channel is tested for the interaction of the boundary layers. The results are reported in Fig 3.10.

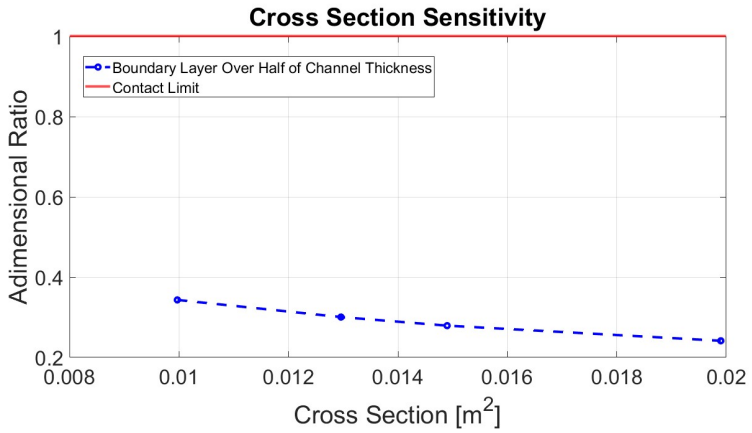

Figure 3.10: Boundary layer analysis: channel cross section

Since by changing the cross section of the channel also the thickness changes, the contact limit is set to one. This is equal to say that the thickness of the boundary layer coincides with half of the thickness of the channel. The analysis is carried evaluating the non dimensional ratio defined as follows:

$$AR_{channel} = \frac{2\delta\left(L\right)}{s} \tag{3.16}$$

Since the thickness of the boundary layer is inversely proportional to the Reynolds number, the wider the cross section area the higher the risk of interaction. The wider the area, the lower the HTF velocity:

$$\delta \sim \frac{1}{Re} \sim \frac{1}{u} \tag{3.17}$$

and

$$u = \frac{\dot{m}}{\rho A_{cross}} \tag{3.18}$$

3.0.5. PCM Containment Model

Since the PCM undergoes phase transition from solid state to liquid state, containment for the slabs is needed to avoid the spilling of the material. This results in additional resistance to the heat interaction between HTF and PCM.
The physical situation can be visualized in Fig 3.11.
The situation reported in Fig 3.11 is the one of the charging of the PCM.

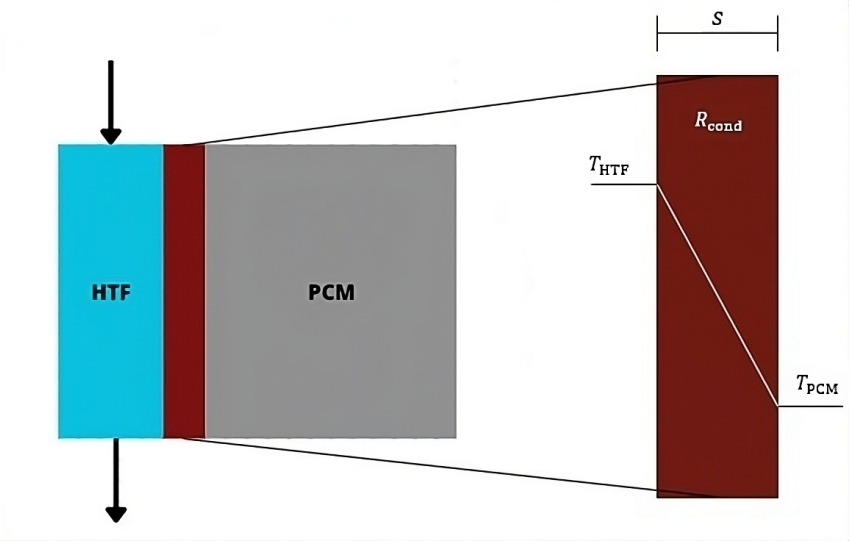

Figure 3.11: PCM containment scheme

As shown, the thermal resistance of the containment results in a decreasing temperature profile. This results in longer charging and discharging times for the slab.
The thermal model for the PCM containment is a conductive thermal resistance:

$$R_{cond} = \frac{t_{enc}}{k_{enc} S} \tag{3.19}$$

where t_{enc} is the thickness of the encapsulation, k_{enc} is the thermal conductivity of the containment material and S is the thermal exchange area.
By employing the electrical analogy, the overall thermal interaction is represented in Fig 3.12.

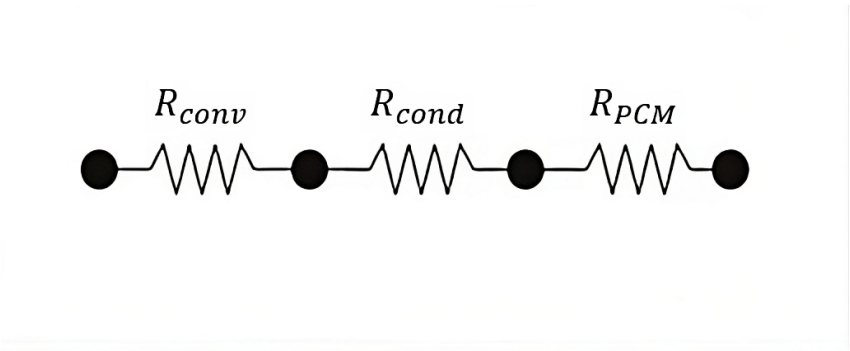

Figure 3.12: Electrical analogy

R_{conv} is the convective thermal resistance in the flow channel, R_{cond} is the conductive thermal resistance of the containment and R_{PCM} is the thermal resistance of internal heat transfer in the slab. The convective thermal resistance is calculated as follows:

$$R_{conv} = \frac{1}{hS} \tag{3.20}$$

where h is the convective heat transfer coefficient determined in eq. 3.11 and S is the thermal exchange area.

4 | Modelica Implementation and Model Validation

Modelica is a powerful, object-oriented, equation-based modeling language designed for simulating complex physical systems across various engineering domains. It is a versatile tool used to model and simulate a wide range of systems, from electrical circuits and mechanical systems to chemical processes and thermal dynamics.
This chapter focuses on the implementation in Modelica of the models that have been presented in chapter 2 and chapter 3. The chapter is organized as follows: firstly, an overview of the Modelica libraries used for the implementation of the LTES model is provided. A simplified single slab storage model and its main components are then presented. The single slab model is then extended to account for the presence of multiple slabs in the storage and the components are changed and adapted. Furthermore, the slab containment and the storage container models are presented. The full storage model is then presented and discussed. Typical storage parameters as the state of charge of the storage are defined and the model is integrated in a heat pump system to simulate realistic operation. Finally, an experimental validation from literature is carried out.

4.0.1. Modelica Libraries

In the context of Modelica, libraries are pre-built collections of reusable components and models that cover specific engineering domains. Modelica libraries are often organized by engineering domains, such as electrical, mechanical, thermal, fluid, control, and more. Each library focuses on a specific domain and contains components tailored to model systems within that domain. Components within Modelica libraries adhere to standardized interfaces, ensuring consistency and compatibility across different models and libraries.
For the LTES, the libraries that have been employed are the following:

- Modelica Thermal.
- Modelica Fluid.

Modelica Thermal

The Modelica Thermal Library focuses on modeling thermal systems and processes, encompassing domains such as heat transfer and thermodynamics. The library includes a wide variety of thermal components, such as heat exchangers, thermal resistors, thermal capacitors, radiators, and more. These components enable users to model heat transfer, thermal storage, and temperature dynamics accurately.
In the LTES, the library has been used to model the following components:

- Heatports to connect elements subjected to heat exchange.
- Thermal conductors to model the conductive heat transfer through the slab containment and the thermal losses through the storage container.
- Convection to model the convective heat transfer between the HTF and the PCM, and the convective thermal losses to the ambient.
- Heat capacitor to model the heat capacity of a component.

Modelica Fluid

The Modelica Fluid Library serves the primary purpose of representing and simulating fluid flow and thermodynamic processes accurately. The library offers a diverse selection of fluid-related components, including pipes, valves, pumps, heat exchangers, and fluid tanks, among others.
In the LTES, the library is used to model the following components:

- Fluidports to connect components in which a fluid flows.
- Pumps.
- Pipes to model the flow channels in the storage.
- Control volume to model the mass of HTF inside the flow channel that exchanges heat with the PCM slab.

The components are employed in the following models.

4.0.2. Single Slab Model

Firstly, a simplified storage model considering only one slab is implemented in Modelica. The block diagram of the storage is reported in Fig 4.1.

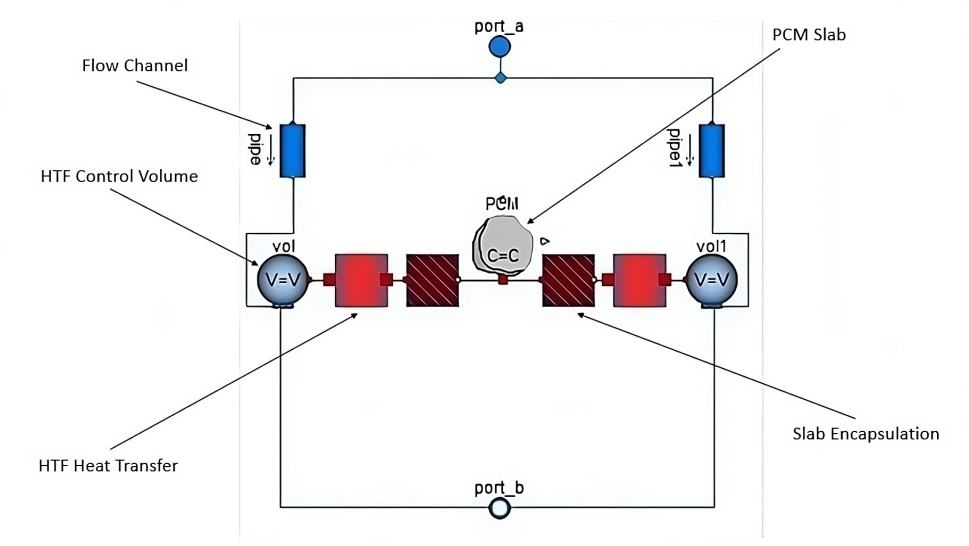

Figure 4.1: Block diagram: single slab storage

This simplified model presents the following assumptions:

- The PCM slab is modelled as a lumped system. This is in contrast with the Biot analysis conducted in chapter 2.
- Thermal losses are neglected.
- The storage container is not considered.

The model is composed of the following blocks, each of which models a physical phenomenon in the storage:

- *port_a* is the inlet port of the storage and the inlet of the HTF.

- *port_ b* is the outlet port of the storage and the outlet of the HTF.
- The two pipes model the HTF flow channels in the storage.
- The HTF control volumes model the volume of HTF in the channels that continuously exchange heat with the PCM slab.
- The HTF heat transfer block models the convective heat exchange between the HTF and the PCM slab.
- The slab encapsulation block models the thermal resistance due to the containment of the slab.
- The PCM slab is modelled as a unique heat capacitor.

The concept behind the HTF control volume comes from the initial conditions of the storage. As discussed in chapter 3, when the storage is not operated, the HTF and PCM are at the same temperature. The control volume models the amount of HTF that fills the channels and, by exchanging heat even when the storage is not operated, thermal equilibrium is reached. When the storage is operated, HTF at the operational temperature enters the storage through *port_ a* and it reaches the control volumes through the pipes. In this way, the control volumes reach the operational temperature. The control volumes allow to account for the transient temperature profile on the HTF side.

4.0.3. HTF Heat Transfer Model

The HTF heat transfer block models the heat that is transferred between the HTF and the PCM slab. In Fig 4.2, the model is reported. The convection component from the Modelica Thermal Library is a model of linear heat convection [42]. It may be used for complicated solid geometries and fluid flow over the solid by determining the convective thermal conductance.

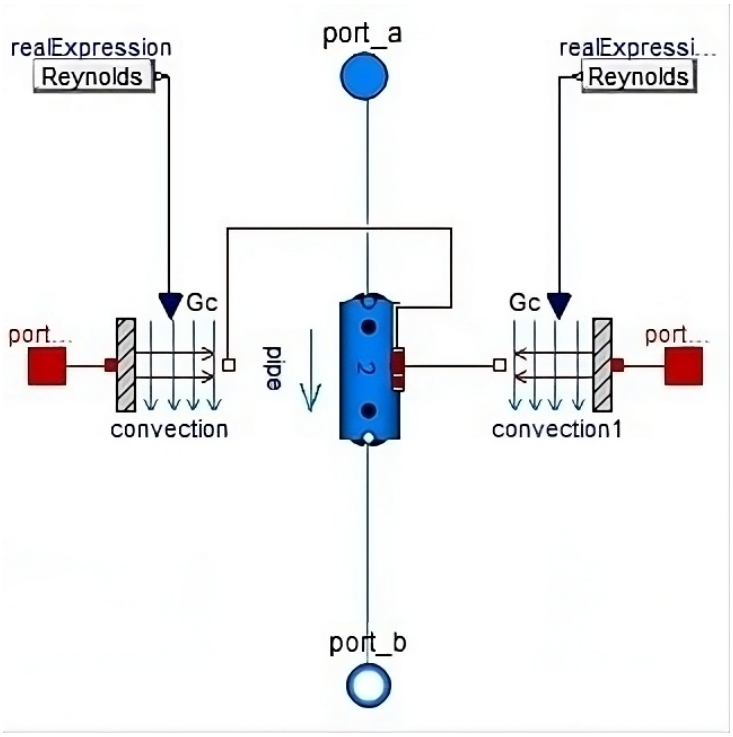

Figure 4.2: HTF heat transfer model

The basic constitutive equation for convection is:

$$Q\_flow = G_C\,(solid.T - fluid.T) \tag{4.1}$$

where Q_flow is the heat flow rate from connector "solid" (e.g. the slab) to connector "fluid" (e.g. the HTF). G_C is calculated as follows:

$$G_C = hS \tag{4.2}$$

where h is the convective heat transfer coefficient and S is the heat exchange area. G_C is an input to the component. This comes from the fact that G_C is almost never constant and it is, indeed, dependent on the fluid-dynamic state of the HTF. The convection component is connected to an input signal in which the algorithm presented in the flowchart 3.4 is coded.
Finally, the temperatures $solid.T$ and $fluid.T$ are determined through the heatport connections.

4.0.4. Slab Encapsulation Model

The slab encapsulation block models the thermal resistance due to the slab containment. The model is reported in Fig 4.3.

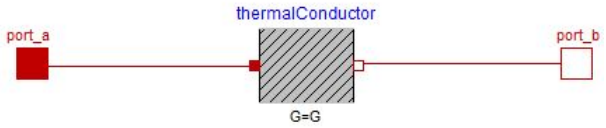

Figure 4.3: Slab encapsulation model

The thermal conductor component models transport of heat without storing it [43]. It may be used for complicated geometries where the thermal conductance G, which is the inverse of the thermal resistance, is assumed to be constant. If the component consists mainly of one type of material and a regular geometry, it may be calculated with the following equations:

$$G = \frac{1}{R_{enc}} = \frac{k_{enc} S}{t_{enc}} \tag{4.3}$$

where k_{enc} is the thermal conductivity of the encapsulating material, t_{enc} is the thickness of the containment wall and S is the heat exchange area.
From the thermal conductance, the model determines the heat transferred as follows:

$$Q\_\ flow = G\,(port\_\ a.T - port\_\ b.T) \tag{4.4}$$

4.0.5. Multiple Slabs Model Extension

The model presented so far only considers the presence of one slab in the storage. The model should be extended to account for the presence of multiple slabs. To do it, in Modelica, a for cycle is employed. The single slab model is composed by:

- One slab.
- Two pipes.

- Two HTF control volumes.
- Two HTF heat interaction blocks.
- Two slab encapsulation blocks.

If the LTES has N PCM slabs, then the full model is considered to have:

- N slabs.
- $N + 1$ pipes.
- $N + 1$ HTF control volumes.
- $2N$ HTF heat interaction blocks.
- $2N$ slab encapsulation blocks.

However, as reported in chapter 4 and shown in Fig 4.2, the extreme slabs are in contact with the HTF only on one side. For this reason, the model components are rearranged as follows:

- N slabs.
- $N - 1$ pipes.
- $N - 1$ HTF control volumes.
- $2N - 2$ HTF heat interaction blocks.
- $2N - 2$ slab encapsulation blocks.

It should be considered that every flow channels exchanges heat with two PCM slabs. This means that every slab is served by 1/2 pipe as well as 1/2 HTF heat interaction block. The slab encapsulation model, instead, is present on each side of the slab. This means that for every slab, two slab encapsulation blocks are considered. This is valid for every slab except the extreme ones. These two slabs are in direct contact with the storage container, and their encapsulation model is different from the others and will be discussed in the next section.
When the number of blocks based on the number of slabs in the storage is defined, extending the model to multiple slabs is simply a matter of connecting the blocks to each others. This can be done employing a for cycle that connects each single slab model to the next one. The connection point is represented by the HTF control volume of the i-th single slab model that exchanges heat also with the (i+1)-th single slab model.

4.0.6. Storage Container Model

The storage container model accounts for the thermal losses to the environment. As previously stated, only the extreme slabs of the storage are in contact with the storage container. The model is composed by two thermal components: the first one is related to the thermal conduction through the storage container, while the second one considers the convective transfer due to ambient air. The model is presented in Fig 4.4.

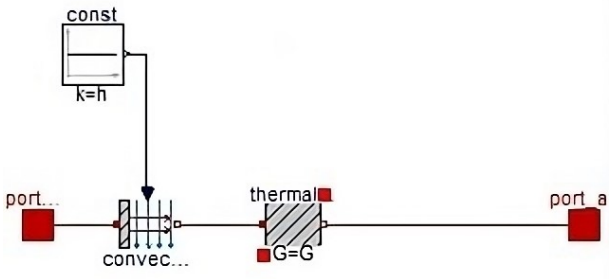

Figure 4.4: Storage container model

The conduction through the container wall is modelled with a thermal conductor, as done for the slab encapsulation model. The convective heat transfer with ambient air is modelled through the convection block, as done for the HTF heat interaction model. Contrary to the HTF heat interaction model, where G_C is determined through an external algorithm, for the heat exchange with the environment it is assumed to be constant. This assumption comes from the fact that the LTES is usually employed indoor, where environmental conditions are not subjected to sudden changes. G_C becomes then an input provided manually by the user.
The thermal losses are calculated as follows:

$$Q\_flow = G_{tot}\,(port\_a.T - port\_b.T) \tag{4.5}$$

where $port\_a.T$ is the extreme slab temperature and $port\_b.T$ is the ambient temperature. G_{tot} is the total thermal conductivity calculated as follows:

$$G_{tot} = G + G_C = \left(\frac{k_{wall}}{t_{wall}} + h_{amb} \right) S \tag{4.6}$$

where k_{wall} is the thermal conductivity of the container material, t_{wall} is the thickness of the container wall, h_{amb} is the convective heat transfer coefficient of ambient air, and S is the heat exchange area.

4.0.7. Full Model

The final LTES model comprehends all the components that have been previously presented. The model is reported in Fig 4.5.

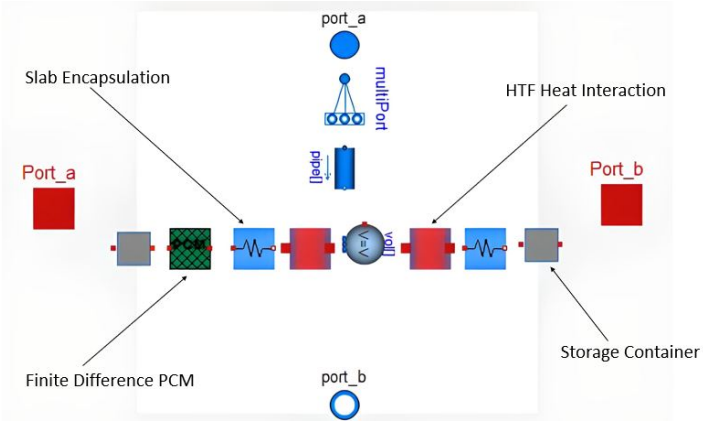

Figure 4.5: Full LTES model

With respect to the single slab model, in the full model the PCM slab is modelled through the finite difference method that has been presented in chapter 3.
Port_ a and Port_ b are used to apply the ambient temperature conditions for the thermal losses.
The multiPort component is employed to split the mass flow rate of the system that enters the storage equally in the flow channels present in the LTES.

4.0.8. State Of Charge

One of the most important parameters when dealing with energy storage technologies is represented by the state of charge (SOC). The SOC is defined as the energy available in the storage at a specific point in time with respect to its capacity [44]. Properly defining it in the model is essential to monitor the charging and discharging phases.

In general, the SOC of an energy storage is defined as follows:

$$SOC = \frac{E_{stored}}{E_{storable}} \tag{4.7}$$

where E_{stored} is the energy that is stored in the storage at a certain time, and $E_{storable}$ is the maximum storable energy. When the storage is fully charged, the SOC is equal to one, while when it is fully discharged the SOC is equal to zero.
When dealing with LTES, the maximum storable energy $E_{storable}$ is defined as the sum of three contributions: the sensible energy stored in the solid phase, the latent energy stored in the phase transition and the sensible energy stored in the liquid phase. From this, the maximum storable energy in a LTES is defined as follows:

$$E_{storable} = \rho\left(T\right) V \left(c_{0,s}\left(\left(T_m - \frac{\Delta T}{2}\right) - T_{min}\right) + \Delta H_m + c_{0,l}\left(T_{max} - \left(T_m - \frac{\Delta T}{2}\right)\right)\right) \tag{4.8}$$

where ρ is the density of the PCM, V is the volume of the storage, $c_{0,s}$ is the specific heat capacity of the PCM in the solid state, $c_{0,l}$ is the specific heat capacity of the PCM in the liquid state, ΔH_m is the enthalpy of phase change, ΔT is the temperature range of phase change, and T_{min} and T_{max} are the minimum and the maximum operative temperatures of the PCM respectively.
Defining the energy stored E_{stored} at a certain point in time is challenging. This comes from the fact that the PCM temperature is not uniform in the space domain, hence different points have different energy contents. For this reason, the energy stored is calculated taking as a reference the average temperature of the PCM:

$$\begin{cases} E_{stored} = \rho\left(T\right) V \left(c_{0,s}\left(\left(T_{mean} - T_{min}\right)\right)\right) & solid \\ E_{stored} = \rho\left(T\right) V \left(c_{0,s}\left(\left(T_m - \frac{\Delta T}{2}\right) - T_{min}\right) + \phi_{mean}\Delta H_m\right) & liquid \\ E_{stored} = \rho\left(T\right) V \left(c_{0,s}\left(\left(T_m - \frac{\Delta T}{2}\right) - T_{min}\right) + \Delta H_m + c_{0,l}\left(T_{mean} - \left(T_m - \frac{\Delta T}{2}\right)\right)\right) & transition \end{cases} \tag{4.9}$$

where T_{mean} is the mean temperature of the storage and phi_{mean} is the mean melt fraction. The mean parameters can be calculated from the finite difference discretization of the storage as follows:

$$\begin{cases} T_{mean} = \frac{\sum_{n=1}^{N} T(n)}{N} \\ \phi_{mean} = \frac{T_{mean} - \left(T_m - \frac{\Delta T}{2}\right)}{\Delta T} \end{cases} \tag{4.10}$$

where N is the number of nodes the LTES is discretized with, and $T\,(n)$ is the temperature of each node.

4.0.9. Integration in Heat Pump System

To simulate the operation of the LTES in a real system, the model is integrated in a heat pump system. The purpose is to investigate the charging time of the storage in a real system operation. The overall heat pump + storage model is shown in Fig 4.6.

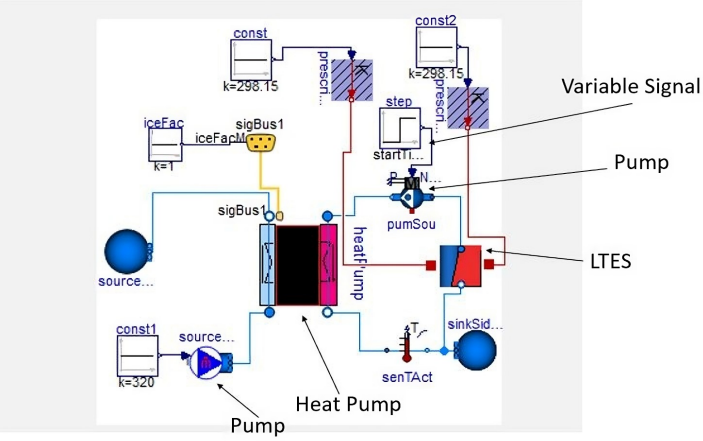

Figure 4.6: Heat pump + LTES

The LTES is inserted in a close circuit with the heat pump. The HTF can only flow from the heat pump to the storage and back. The model is equipped with two pumps: the first one is on the side of the condenser, while the second one is on the evaporator circuit. The speed of the evaporator pump can be regulated with the outside input. This allows to simulate a realistic operation, where the storage is not used all the time and the HTF does not continuously flow in the circuit. The pump can be set to work for a certain time, and then stop when the storage is fully charged. When the pump is stopped, the SOC of the storage decreases due to the thermal losses through the walls.
Two temperature blocks are connected to the storage. These specify the ambient temperature, and are used to compute the thermal losses of the storage.
An exemplary case is run to simulate a realistic operation of the LTES. The specification

of the PCM and storage are reported in table 4.1 and 4.2 respectively.

PCM	n-octadecane
Density $[kg/m^3]$	772
Melting Temperature $[C]$	28.2
Viscosity $[kg/ms]$	0.005
Specific Heat Capacity $[kJ/kgK]$	2.330
Thermal Conductivity $[W/mK]$	0.1505
Latent Heat of Fusion $[kJ/kg]$	243.5
Thermal Expansion Coefficient $[K^{-1}]$	0.00091

Table 4.1: PCM specifications

Number of Slabs	5
Slab Length $[m]$	0.3
Slab Width $[m]$	0.074
Slab Thickness $[m]$	0.02
Flow Channel Thickness $[m]$	0.005
Encapsulation Material	Stainless Steel
Stainless Steel Thermal Conductivity $[W/mK]$	15
Storage Container Material	Perspex
Perspex Thermal Conductivity $[W/mK]$	0.2

Table 4.2: Storage specifications

The considered PCM is n-octadecane, which is an alkane hydrocarbon which is solid at room temperature [40]. For this reason, it is particularly suitable for low temperature LTES applications.

When dealing with a storage that has n slabs, the SOC is calculated as in eq. 4.9. In this case, the mean temperature that is considered is the mean of the mean temperatures of the slabs:

$$T_{mean,storage} = \frac{\sum_{i=1}^{n} T(i)}{n} \tag{4.11}$$

where $T(i)$ is the mean temperature of the i-th slab, and n is the number of slabs in the storage.

The system is simulated for seven hours to analyze the charging time of the storage. The

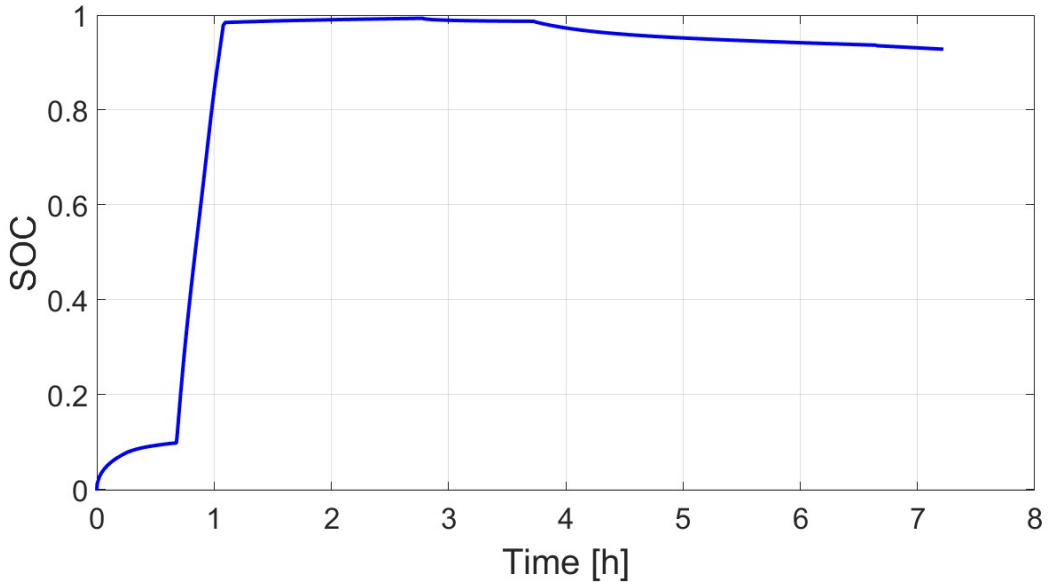

Figure 4.7: State of charge

results are reported in Fig 4.7.
The results show that it takes one hour to reach 100% of SOC. In the graph, it is possible to see two different trends in the charging process. At first, the PCM is in the solid state, and the energy content is reached through sensible energy. The increase in the slope of the charging process comes from the latent heat of fusion. The highest energy content of the storage, in fact, stands in the enthalpy of phase transition. For this particular case, the charging process stops when the PCM is fully melted. When the circulating pump is stopped, the SOC starts decreasing due to the thermal losses. As expected, due to the very low thermal conductivity of the PCM, and due to the phase change at almost constant temperature, thermal losses are not very relevant. The SOC takes almost four hours to decrease from 100% to 95%.

4.0.10. Experimental Validation

To validate the Modelica model of the LTES, experimental results from literature have been replicated. In particular, the experiment that has been replicated was developed by Gurel et al. [41].
The authors developed a flat plate latent thermal energy storage. The Heat Exchanger unit was designed as shown in Fig. 4.8 and 4.9. In the analysis, n-octadecane was used as the PCM, while water was used as the HTF. The plate material between the PCM and HTF was steel, and the material shell of the plate heat exchanger LHTES system was Perspex.

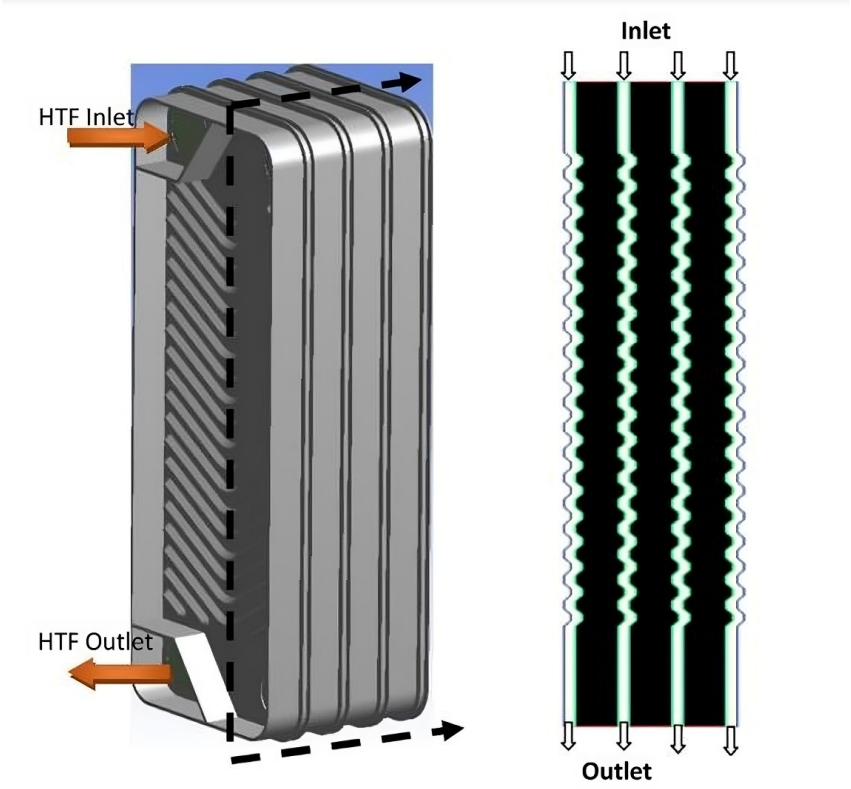

Figure 4.8: LTES deign

The properties of n-octadecane are the same as the ones reported in Table 4.1. The storage properties are instead reported in Table 4.3. The study reported the results for

Number of Slabs	3
Slab Length $[m]$	0.192
Slab Width $[m]$	0.074
Slab Thickness $[m]$	0.0113
Flow Channel Thickness $[m]$	0.0025
Encapsulation Material	Steel
Steel Thermal Conductivity $[W/mK]$	45
Storage Container Material	Perspex
Perspex Thermal Conductivity $[W/mK]$	0.2

Table 4.3: Storage specifications

different HTF inlet temperatures in the storage. In particular, 62 °C, 57 °C and 52 °C have been considered.

The storage specifications are inserted in the Modelica model, and the results are compared. The results that are compared are the mean temperatures of the storage for different inlet temperature of the HTF. The result are reported in Fig 4.10.

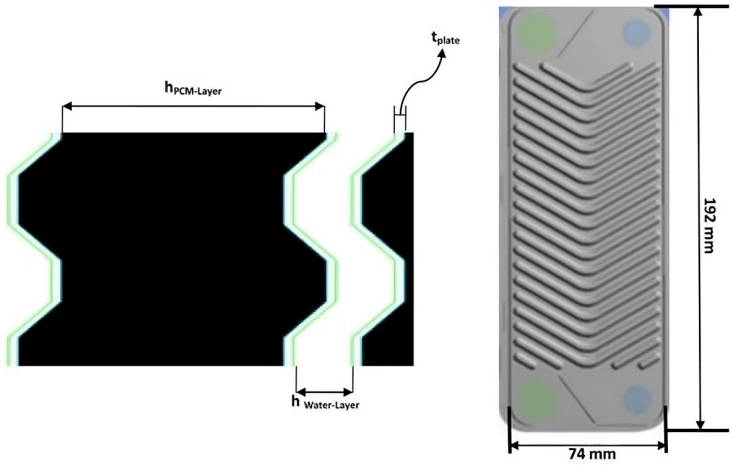

Figure 4.9: LTES design particular

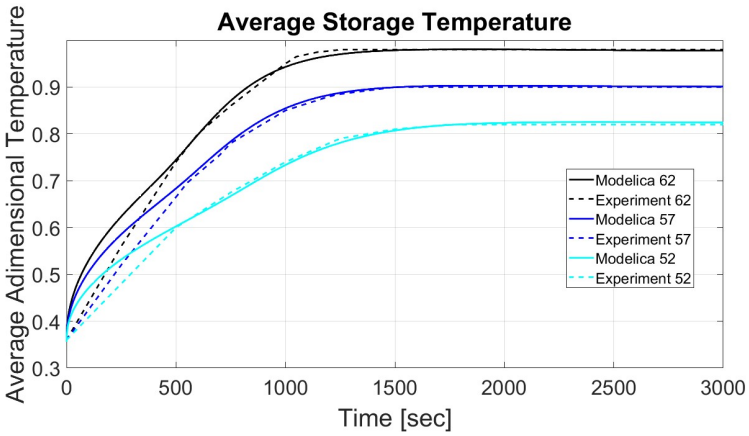

Figure 4.10: Experimental validation: mean storage temperature as a function of time

The results show that the temperature trends are very close to the experimental ones. For all cases, the highest difference in the trend is reached in the initial periods of charging. It should be noted that in the study it is not specified how the average temperature of the storage is determined. The average storage temperature for the Modelica model is calculated as the arithmetic mean of the temperature of each node of the 2D grid PCM at each time of the simulation.

To better visualize the deviation of the profiles, the errors are reported in Fig 4.11. The error is computed as:

$$e = \left| \frac{T_{model} - T_{experimet}}{T_{experiment}} \right| * 100 \tag{4.12}$$

where T represents the temperature of the storage for each considered case.

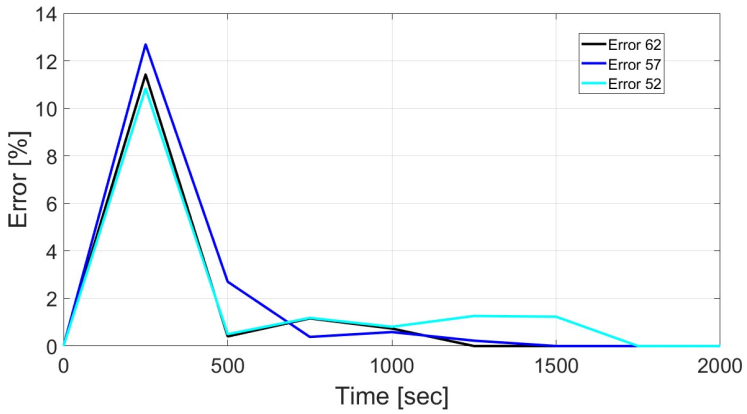

Figure 4.11: Experimental validation: model error

The graph shows that the highest error is in the initial times of charging. The error never overcomes 13%. However, it converges quickly to very low values. The very low error is considered as a validation of the Modelica model.

5 | Conclusion

The aim of this thesis is to develop guidelines for the modelling of latent thermal energy storage (LTES) in object oriented programs such as Modelica. The work is developed for the slab LTES. This is a particular design of the storage where the phase change material (PCM) is contained in flat plate containers, and the heat transfer fluid (HTF), that exchanges heat with the PCM, flows in the channels between neighbouring slabs.
The model that is implemented in Modelica can essentially be divided in three domains: the heat interaction between the HTF and the PCM, the PCM internal heat transfer and the storage thermal losses.
The heat that is exchanged between the HTF and the PCM is determined through the calculation of the convective heat transfer coefficient. Its value is obtained through a fluid-dynamic analysis of the HTF flow in the channel. The analysis considers the HTF properties, the channel geometry and whether the flow is laminar or turbulent. The correct correlations for determining the convective heat transfer coefficient are then applied. Furthermore, the model is also able to check whether the interaction between the boundary layers in the flow channels occurs, to account for velocity altering effects.
The internal heat transfer model deals with the complexity of the phase change. Heat transfer with phase transition from solid to liquid state involves the problem of tracking the motion of the solid-liquid interface as a function of time. The solution requires solving a complex set of partial differential equations (PDE). Object oriented programs are not supposed to solve PDEs, but only ordinary differential equations (ODEs) instead. For this reason, simpler approaches are investigated. Firstly, a Biot analysis is conducted and the results show that due to its extremely low thermal conductivity, the PCM cannot be modelled as a concentrated parameter. The PCM space domain is then dicretized with a 2D finite difference scheme, and the internal heat transfer is solved by employing a conduction model. The model is validated against CFD simulations carried in Ansys Fluent. Several simulations are done for different slab geometries in order to understand the impact of the dimensions. The results show that while the height of the slabs does not have a relevant impact, the thicker the slab the more the deviation between Modelica and CFD. This comes from the fact that the Modelica model does not consider the impact of

natural convection during phase change, while CFD does. The issue is solved by developing a fictive thermal conductivity of the PCM. This considers an enhancement coefficient for the thermal conductivity of the material during phase change. The enhancement coefficient is calculated as the ration of the internal energy of the PCM in the case natural convection is accounted for and the case in which it is not. The comparison between the results of the enhanced Modelica model and CFD shows a reduced error.
The thermal losses are considered through the storage container. They model accounts for the conductive heat transfer through the container walls and the convective heat transfer due to ambient air. Since the LTES is usually employed indoor, and since the highest energy content is at almost constant temperature, thermal losses turn out to have low impact on the performance of the storage.
The implementation of the model in Modelica is conducted employing the main components of the Modelica Thermal and Modelica Fluid libraries, that are the most used to model thermal and fluid dynamic problems. The model is then inserted in a heat pump system to simulate realistic operations. The simulation is run for eight hours and with very little computational time. This overcomes one of the main problems of modelling a phenomenon that is described by partial differential equations. The fictive thermal conductivity model is able to reproduce accurately the results from CFD but with little computational cost. This shows that the model can be used to develop control strategies of systems that have to run for long times.
Finally, the model is validated with an experimental study from literature. The parameters of the experiment have been exactly replicated in the model, and the mean temperatures of the storage have been compared. To generalize the results, the storage has been simulated for different inlet temperatures of the HTF. The results show that the temperature profiles are very similar to the ones from literature. Indeed, the temperature error never overcomes 12%. The differences have to be searched in modelling assumptions that the experiment is able to account for.
This thesis work was able to couple object oriented modelling and CFD simulations to replicate a complex phenomenon such as the one of heat transfer with phase change with a simplified approach, but with an acceptable level of accuracy. CFD tuned out to be an extremely powerful tool to be fully aware of the consequences of making particular assumptions when developing simplified modelling approaches.
Future work should consider applying the developed guidelines when modelling LTES, to insert it in wider energy systems and develop accurate control strategies and energy management techniques.

BIBLIOGRAPHY

(1) Gur M. Review of electrical energy storage technologies, materials and systems: challenges and prospects for large-scale grid storage

(2) Leonard Wagner. Overview of energy storage methods, December 2007.

(3) Sergio Vasquez, Energy Storage Systems for Transport and Grid Applications

(4) Om Krishan, An updated review of energy storage systems: Classification and applications in distributed generation power systems incorporating renewable energy resources,

(5) Shafiqur Rehman. Pumped hydro energy storage system: A technological review. (2014)

(6) Haisheng Chen, Progress in electrical energy storage system: A critical review

(7) Mark Dooner, 14 - Compressed-Air Energy Storage

(8) Shripad Revankar, Chapter Six - Chemical Energy Storage

(9) Atul Sharma, Review on thermal energy storage with phase change

materials and applications

(10) Mukrimin Sevket Guney, Classification and assessment of energy storage systems

(11) https://onlinelibrary.wiley.com/doi/abs/10.1002/er.5057

(12) Conrado Ermel, Thermal storage integrated into air-source heat pumps to leverage building

electrification: A systematic literature review

(13) Jianghong Wu, All-weather characteristic studies of a direct expansion solar integrated air

source heat pump system based on PCMs

(14) Minglu Qu, An Experimental Study on the Improvement of Reverse Cycle

Defrosting Performances for a Cascade Air Source Heat Pump using

Thermal Energy Storage Based Defrosting Method

(15) Zhang Long, A novel defrosting method using heat energy dissipated

by the compressor of an air source heat pump

(16) Sandra Raquel Leite da Cunha, Phase change materials and energy efficiency of buildings: A review of

knowledge

(17) Michelle K. DeValeria, Energy and thermal storage in clusters of grid-independent buildings

(18) https://ease-storage.eu/wp-content/uploads/2015/10/EASE-EERA-recommendations-Roadmap-LR.pdf

(19) Zakir Khan, A review of performance enhancement of PCM based latent heat storage

system within the context of materials, thermal stability and

compatibility

(20) https://www.researchgate.net/publication/331856541_A_comprehensive_review_of_recent_advances_\\in_materials_aspects_of_phase_change_materials_in_thermal_energy_storage

(21) C. Veerakumar, Phase change material based cold thermal

energy storage: Materials, techniques and

applications – A review

(22) Nelson O. Moraga, Cooling Li-ion batteries of racing solar car by using multiple phase

change materials

(23) Siddique A. Khateeb, Thermal management of Li-ion battery with phase change material

for electric scooters: experimental validation

(24) https://www.sciencedirect.com/science/article/abs/pii/S1270963812000892

(25) https://www.sciencedirect.com/science/article/pii/S1364032106001651

(26) https://www.semanticscholar.org/paper/Finite-element-analysis-of-cyclic-heat-transfer-in-Gong-Mujumdar/d874a6684c7d7e41531e04b499fd19dba42126ba

(27)https://www.researchgate.net/publication/245212939_Analysis_and_modeling_of_a_phase_change_storage_system_for_air_conditioning_applications

(28) https://www.researchgate.net/publication/223599229_Modeling_and_simulation_on_the_thermal_performance_of_shape-stabilized_phase_change_material_floor_used_in_passive_solar_buildings

(29) https://www.scirp.org/(S(i43dyn45teexjx455qlt3d2q))/reference/ReferencesPapers.aspx?ReferenceID=1233693

(30) https://www.tandfonline.com/doi/abs/10.1080/10407799008961737

(31) https://www.researchgate.net/publication/223844452_\\Mathematical_modelling_of_PCM_air_heat_exchanger

(32) https://www.researchgate.net/publication/245367841_Thermal_Analysis_of_Composite_Phase_Change_Drywall_Systems

(33) Dre Helmns, Development and Validation of a Latent Thermal Energy

Storage Model Using Modelica

(34) file:///C:/Users/Marco/AppData/Local/Temp/BS2019_211148

(35) Mustafa S. Mahd, Natural convection improvement of PCM melting in partition latent heat

energy storage: Numerical study with experimental validation

(36) http://www.fluiddynamics.it/capitoli/blas.pdf

(37) https://www.univpm.it/Entra/Engine/RAServeFile.php/f/P001087/allegati_doc/convezione.pdf

(38) https://resources.system-analysis.cadence.com/blog/\\msa2022-velocity-and-thermal-boundary-layers-for-fluid-dynamics

(39) https://farside.ph.utexas.edu/teaching/336L/Fluidhtml/node113.html

(40) https://pubchem.ncbi.nlm.nih.gov/compound/Octadecane

(41) Barı ¸s GÜREL, A numerical investigation of the melting heat transfer characteristics

of phase change materials in different plate heat exchanger (latent

heat thermal energy storage) systems

(42) https://build.openmodelica.org/Documentation/Modelica.Thermal.HeatTransfer.Components.Convection

(43) https://www.maplesoft.com/documentation_center/online_manuals/modelica/Modelica_Thermal_HeatTransfer_Components.html

(44) https://www.techtarget.com/whatis/definition/state-of-charge-SOC